Experimental Techniques (2024) 48:501–522
https://doi.org/10.1007/s40799-023-00676-8

RESEARCH PAPER

A Numerical Prediction for Hole-Splitting Damage of DP Steels Based on Plastic Work Criterion Using a Polynomial Stress Potential

M. Firat[1] · T. A. Akşen[1] · B. Şener[2] · E. Esener[3]

Received: 22 September 2022 / Accepted: 1 September 2023 / Published online: 26 September 2023

Abstract

The main purpose of this study is to exhibit failure prediction capability of polynomial-based yield functions with a basic damage model. For this purpose, a constitutive model considering anisotropic plasticity and ductile fracture was developed. In this model, anisotropic plastic behavior of dual phase steels, namely DP600 and DP800, was described by quadratic Hill48 and non-quadratic anisotropic homogeneous the fourth-order polynomial (HomPol4) stress potentials and the generalized plastic work criterion from ductile damage models was used for the prediction of fracture initiation. The model has been implemented into an implicit finite element (FE) code. The parameters of the constitutive model were calibrated with uniaxial tensile tests performed in different directions with respect to the rolling direction of the materials and anisotropic stress potentials were evaluated by comparison of the predicted in-plane variations of the plastic properties (yield stress ratios and Lankford coefficients), and yield locus contours with experimental data. The calibrated model was firstly applied to uniaxial tensile test and then to a hole expansion test to predict fracture. The stroke values at fracture, hole expansion ratios (HER) and fracture locations were investigated. Any significant difference between the anisotropic stress potentials was not observed in terms of HER predictions, however plastic work criterion in conjunction with HomPol4 function predicted the crack initiation locations accurately on the fractured samples. Afterward, the Lode parameter and stress triaxiality effects were investigated in fracture stroke prediction. Since the HomPol4 predictions of fracture initiation locations are accurate, the predicted HomPol4 results from the generalized plastic work criterion were compared with the modified Mohr-Coulomb ductile fracture model results. A significant improvement was observed in the fracture displacement predictions. However, it is seen that the failure location predictions of both models were the same. From these results, it can be concluded that the HomPol4 yield criterion has an effective potential to predict the failure locations even though with a basic damage model. In the current study, the out-of-plane anisotropy effect was assessed as well. To this end, Hill48's parameter correlated with the out-of-plane shear components were adjusted. It was found that the out-of-plane anisotropy has a negligible effect on the predictions of HER and fracture initiation location.

Keywords Hole-splitting · Dual phase steel · Anisotropic plasticity · Implicit method · Fracture location

Introduction

In order to decrease the issues of fuel consumption and air pollution, several alternative materials have been continuously developed in the automotive industry. Among them, advanced high strength steels (AHSS) are prominent materials due to their high strengths and strain hardening capabilities. These properties enable engineers to manufacture lightweight vehicles with high crash performance. Although AHSS have superior properties, edge fracture phenomenon is frequently observed in these steels during stretch-flanging process used in manufacturing of several parts such as door outer panel, control arms, cross members etc. [1]. Therefore,

✉ M. Firat
firat@sakarya.edu.tr

[1] Department of Mechanical Engineering, The University of Sakarya, Sakarya 54187, Turkey

[2] Department of Mechanical Engineering, Yildiz Technical University, Istanbul 34349, Turkey

[3] Department of Mechanical Engineering, Bilecik Seyh Edebali University, Bilecik 11230, Turkey

it has been crucial to predict edge fracture of AHSS in the automotive industry. Although uniaxial tensile test (UTT) could ascertain mechanical behavior of materials, it is inadequate to provide information about the stretch-flangeability. Edge stretchability of materials has been evaluated by hole expansion test (HET). In this test, a hole is made by punching or machining processes on the sheet, then it is expanded by a punch until the onset of edge fracture [2].

HET can be conducted using a standard conical punch, flat bottom punch, or hemispherical punch. In all methods, the deformation path is different from each other. In conical punch, the deformation path is roughly similar to the uniaxial tension conditions along the radial direction of the deformed sample. For the flat bottom punch and the hemispherical punch, although the deformation mode is uniaxial tension at the hole edge, it rapidly changes to plane strain in a narrow range [3]. Besides, in the report of Sadagopan et al. [4], the HETs conducted using conical and flat-bottom punches were separately investigated. The formability limit obtained by a conical punch was found to be higher than the flat-bottom punch configuration. In the report, the reason for this situation was attributed to the different strain paths, which is also consistent with the work of Paul [3]. In addition, it is emphasized in the related report that the conical punch configuration is more simulative and suitable for production. Paul [3] also reported that only the conical punch configuration provides the true stretch formability limit of the sheets.

The hole expansion ratio (HER) is the fundamental parameter obtained from the aforementioned HETs. Expansion in the hole diameter is considered as an indicator of the edge formability, and the ratio of the diameter after test to initial hole diameter is called as HER.

In the literature, several studies have been performed focusing on the prediction of HER. In a part of these studies, researchers have attempted to determine a relationship between HER and mechanical properties of the materials by using regression techniques. Chatterjee and Bhadeshia [5] investigated the stretch-flangeability of the steels with different microstructures and determined that HER decreases linearly as the increase of ultimate tensile strength (UTS) of the materials. However, Hance [6] carried out a study with 980 MPa steel grades and determined that although the investigated steels have the same UTS values, they exhibit different edge stretchability performances based on the classification system developed in the study. Heibel et al. [7] found a strong correlation between HER and the true thickness strain value at fracture obtained from the tensile test. They introduced it as an index for assessing the local formability of a wide range of AHSS. Larour et al. [8] showed that the parameters (the area reduction and minimum thickness at fracture) obtained from the punched tensile test specimen better represent the edge crack sensitivity of AHSS grades than EDM or milled specimen. Fang et al. [9] carried out on an experimental study on C-Mn steels and found that the ratio of yield stress to UTS has positive effect on HER. Yoon et al. [10] studied hole-flangeability of a low carbon steel, 304 stainless steel and TWIP steel. Researchers indicated that HER increases as strain rate sensitivity of the materials increases. Adamczyk and Michal [11] conducted HET on high strength steels (HSS) and derived an analytical expression for HER is based on average anisotropy coefficient (r_m) and total elongation of the materials. Then, Comstock et al. [12] expanded the study of Adamczyk and Michal for different materials and edge conditions. They also considered the effect of thickness and strain hardening exponent on the prediction of HER. Unlike these studies, Paul [13] derived a nonlinear equation between HER and mechanical properties (UTS, r_m and the percentage total elongation). In addition to mechanical properties, hole-cutting methods and the parameters related to the shearing process also effect the HER value. Larour et al. [14] compared the HER values of the drilled and punched specimens for AHSS. They investigated the effect of numerous factors (cutting clearance, tool geometry, and wear in punch and die) regarding the shearing process. Researchers determined the optimum cutting clearance value for AHSS and found a linear correlation between the ratio of burnish to fracture from the sheared edge parameters and HER. Besides, the maximum HER value was obtained with orthogonal cutting punch geometry (ISO standard) compared to the other geometries (convex and concave) due to the uniform cutting clearance along the hole perimeter. Although the abovementioned studies give consistent results related to the prediction of HER, the developed equations are empirical, and their usage are limited. Therefore, application of a generalized methodology is required for the prediction of HER. From this viewpoint, computer modeling and various numerical methods are applied on the solving of different engineering problems by several scientists [15–19]. Among the numerical methods, the finite element method is the most preferred technique in the metal forming industry. Definition of plastic behavior of the material is an indispensable in FE modelling of a process and determination of a proper stress potential for material has a profound effect in terms of reliability of FE analyses. This phenomenon has been studied for HET by various researchers. Kuwabara et al. [20] studied the plastic behavior of a dual-phase steel sheet (DP780) during HET and performed FE analyses of the test with three different stress potentials (von Mises, Hill48 and Yld2000-2d). They compared the numerical and experimental thickness distributions along both the hole edge and radial directions of the part and declared that the most compatible results were obtained with Yld2000-2d criterion. A similar study was performed by Iizuka et al. [21] for a HSS sheet and the most successful results were obtained with same yield criterion. Kuwabara et al. [22] modeled the anisotropic behaviors of AA6016-O and AA6016-T4 aluminum alloys by Yld2000-2d and different hardening laws. They determined that thickness distribution profiles could

better predicted with anisotropic hardening law for AA6016-O alloy. Lee et al. [23] investigated the effect of both yield criteria and parameter optimization on hole expansion simulation. They applied Yld2000-2d and Yld2004-18p yield criteria and determined that the prediction accuracy of FE analyses highly depend on the parameter identification. Korkolis et al. [24], Ha and Korkolis [25] calibrated Yld2000-2d coefficients with uniaxial and plane strain tension tests for AA6022-T4 aluminum alloy and obtained significant enhancements in the thinning predictions by including anisotropic behavior in plane strain stress state. In these studies, researchers focused on thinning predictions in the HET, whereas they didn't give the detailed information about the prediction of HER. In order to predict HER, application of a failure criterion coupled with FE analysis is required. Chung et al. [26] applied a stress triaxiality-based failure criterion as well as Hill48 anisotropic criterion to HET of TWIP940, TRIP590 and R340 steels and predicted HERs of these materials. Takuda et al. [27] investigated the forming limit of a mild steel and two types of HSS. They applied Cockcroft and Latham ductile damage model combined with Hill48 yield function and predicted HERs of these materials. Yoon et al. [28] applied a different method to predict HER. They considered fracture toughness of the materials and predicted HERs by applying a strain-based fracture criterion along with Hill48 yield criterion. Chinara et al. [29] described the anisotropic behavior of DP590 steel with Hill48 stress potential and applied a strain-based failure criterion in order to predict HER. Mu et al. [30] used three uncoupled ductile fracture criteria, namely Lou-Huh [31], Oh [32] and Brozzo [33], to predict HER of DP780 steel and reported that the best predictions were achieved by the Lou-Huh model. In these studies, scientists accurately predicted HERs of the materials with anisotropic material models and ductile fracture criteria. However, it should be emphasized that anisotropic stress potentials have effect on the prediction of the not only HER but also fracture location and this phenomenon needs further detailed investigation at the material locations prone cracking. In addition, as it is seen from the literature review, linear transformation based anisotropic material models, namely Yld2000-2d or Yld2004-18p, have been widely used to model material anisotropy in the studies. These functions are convex and have powerful modeling capability. However, computations of their first and second order gradients are difficult, and they have highly nonlinear formulas in the parameter identification. When compared with linear transformation-based models, polynomial yield functions have simpler and generalized structure and also their derivatives could be easily computed, therefore they could be easily implemented into any FE software. When considered from this point of view, extension of their range of applications and evaluation of their modeling capability have great importance in the literature.

In this article, the effect of material anisotropy on the prediction of both HER and edge fracture location was investigated. For this purpose, a constitutive model that considers material anisotropy and damage was developed. The study consists of two stages. In the first stage, two anisotropic stress potentials (the quadratic Hill48 and non-quadratic homogeneous polynomial functions) and a basic ductile fracture criterion were used. The functions along with the ductile fracture criterion were separately applied to investigate the effect of different anisotropic stress potentials on fracture prediction. In the second stage, an advanced ductile fracture model considering stress triaxiality and Lode angle was included, and the differences between the predictions of damage models were investigated. Application of the constitutive model was firstly performed on UTT and then on HET. DP steels from the AHSS family were selected. Fracture displacements, HERs and fracture locations of the materials were predicted with the selected stress functions and the numerical results were compared with experiments.

The present study is divided into six sections: In the second section, the developed constitutive model and its components are briefly introduced. In the third section, experimental studies which were performed within the scope of the work are explained. In the fourth section, calibration of the constitutive model parameters is discussed, and functions are evaluated. In the fifth section, applications of the constitutive model, the predicted results from model and comparisons with experiments are presented. Finally, In the sixth section, main conclusions obtained from the study are highlighted.

Constitutive Model

In the present study, a constitutive model that considers material anisotropy and damage was performed. Two anisotropic stress potentials, a basic and an advanced ductile fracture criteria were used in the developed model. In this section, the theory of the selected yield criteria and ductile fracture models are briefly explained.

Anisotropic Stress Potentials

The yield criterion is an important step in the plasticity model definition. The bounds of the onset of the plastic deformation in 3D stress space is characterized by the yield surface, which is described by the yield criterion. The generalized form of the yield criterion is given below.

$$f = \overline{\sigma}\left(\sigma_{ij}\right) - \sigma_0\left(\overline{\epsilon}_p\right) \tag{1}$$

Where, f denotes yield function, $\overline{\sigma}$ is equivalent stress and σ_0 is yield stress of the material, respectively. As yield criteria, quadratic Hill48 and non-quadratic homogeneous

the fourth-order polynomial yield functions were applied to reproduce anisotropic behaviors of two DP sheets (DP600 and DP800). Their formulations and the coefficient identification procedures are given below:

Hill48 stress potential

The first anisotropic stress potential was proposed by Hill [34] and this criterion is broadly employed for the characterization of the steels [26, 35] and some alloys [36]. For general 3-D stress state, the function could be written as the following form:

$$\overline{\sigma}_{\mathrm{Hill48}} = \sqrt{\mathrm{F}\left(\sigma_{yy}-\sigma_{zz}\right)^2 + \mathrm{G}\left(\sigma_{zz}-\sigma_{xx}\right)^2 + \mathrm{H}\left(\sigma_{xx}-\sigma_{yy}\right)^2 + 2\mathrm{L}\tau_{yz}{}^2 + 2\mathrm{M}\tau_{zx}{}^2 + 2\mathrm{N}\tau_{xy}{}^2} \tag{2}$$

In the equation above, F, G, H, L, M and N are the material constants. These parameters could be calibrated with either stress ratios or Lankford coefficients (r values). In this study, an identification based on r values was preferred and the model parameters for both materials were determined by using following equations:

$$\mathrm{F} = \frac{\mathrm{r}_0}{\mathrm{r}_{90}(1+\mathrm{r}_0)}, \mathrm{G} = \frac{1}{1+\mathrm{r}_0}, \mathrm{H} = \frac{\mathrm{r}_0}{1+\mathrm{r}_0}, \mathrm{N} = \frac{(\mathrm{r}_0+\mathrm{r}_{90})(1+2\mathrm{r}_{45})}{2\mathrm{r}_{90}(1+\mathrm{r}_0)} \tag{3}$$

As it is seen from Eq. (3), the constants are determined with Lankford coefficients in rolling (RD), diagonal (DD) and transverse directions (TD) which are denoted by r_0, r_{45} and r_{90}.

The fourth-order homogeneous polynomial stress potential

In the present work, the fourth-order homogeneous polynomial anisotropic stress potential (HomPol4) from non-quadratic criteria was used. HomPol4 stress potential was proposed by Soare et al. [37] and it can be written as following equation:

$$\begin{aligned}\overline{\sigma}^{4(2\mathrm{D})}_{\mathrm{HomPol4}} &= \mathrm{a}_1\sigma_{xx}^4 + \mathrm{a}_2\sigma_{yy}\sigma_{xx}^3 + \mathrm{a}_3\sigma_{yy}^2\sigma_{xx}^2 + \mathrm{a}_4\sigma_{xx}\sigma_{yy}^3 \\ &+ \mathrm{a}_5\sigma_{yy}^4 + \tau_{xy}{}^2\left(\mathrm{a}_6\sigma_{xx}^2 + \mathrm{a}_7\sigma_{xx}\sigma_{yy} + \mathrm{a}_8\sigma_{yy}^2\right) + \mathrm{a}_9\tau_{xy}^4\end{aligned} \tag{4}$$

Soare et al. considered convexity issue in the parameter identification. They introduced constraints on the parameters to acquire a convex yield locus. According to the identification procedure, the first five coefficients could be directly calculated that the equations are given below:

$$\begin{aligned}&\mathrm{a}_1 = 1, \mathrm{a}_2 = -\frac{4\mathrm{r}_0}{(1+\mathrm{r}_0)}, \mathrm{a}_3 = \left(\frac{1}{\overline{\sigma}_{\mathrm{b}}^4}\right) \\ &-(\mathrm{a}_1+\mathrm{a}_2+\mathrm{a}_4+\mathrm{a}_5), a_5 \\ &= \frac{1}{\overline{\sigma}_{90}^4}, a_4 = -\frac{4a_5r_{90}}{(1+r_{90})}\end{aligned} \tag{5}$$

The coefficients a_6 and a_8 are obtained by the optimization of an objective function given in Eq. (6). This function is defined as the sum of squared deviations between the predicted and experimental values of yield stress ratios and Lankford coefficients at interval angles.

$$\mathrm{E} = \frac{1}{2}\sum_{\mathrm{i}=1}^{2}\left[\mathrm{w}_1^{(\mathrm{i})}\left(\mathrm{r}_{\theta,\mathrm{prediction}}^{(\mathrm{i})} - \mathrm{r}_{\theta,\mathrm{exp}}^{(\mathrm{i})}\right)^2 + \mathrm{w}_2^{(\mathrm{i})}\left(\sigma_{\theta,\mathrm{prediction}}^{(\mathrm{i})} - \sigma_{\theta,\mathrm{exp}}^{(\mathrm{i})}\right)^2\right] \tag{6}$$

Where, w_1 and w_2 are the weight functions for r values and yield stress ratios, respectively. 15^0 and 75^0 were chosen as interval angles. In this study, the least square method was used to minimize the objective function. The remaining two coefficients a_7 and a_9 are determined with the equations given below:

$$\mathrm{a}_7 = \left(\frac{2}{(1+r_{45})\overline{\sigma}_{45}^4} - \frac{2}{\overline{\sigma}_{\mathrm{b}}^4}\right) - (a_6+a_8), \mathrm{a}_9 = \frac{\left(\frac{2}{\overline{\sigma}_{45}}\right)^4\mathrm{r}_{45}}{1+\mathrm{r}_{45}} + \left(\frac{1}{\overline{\sigma}_{\mathrm{b}}}\right)^4 \tag{7}$$

Eleven mechanical parameters such as yield stress ratios and r-values at 0^0, 15^0, 45^0, 75^0 and 90^0 and as well as yield stress ratio at equi-biaxial stress state $\left(\overline{\sigma}_b\right)$ are required to determine the model parameters. In original, the HomPol4 criterion is applicable for plane stress conditions. In this study, HomPol4 criterion was generalized for 3D stress space in order to include the effect of out of plane stresses. The 3D form of HomPol4 criterion is given in Eq. (8).

$$\begin{aligned}&\overline{\sigma}_{HomPol4}{}^{(3D)}(\sigma_{xx},\sigma_{yy},\sigma_{zz},\tau_{xy},\tau_{yz},\tau_{zx}) \\ &= \sqrt{\overline{\sigma}^{2(2\mathrm{D})}_{\mathrm{HomPol4}}(\sigma_{xx}-\sigma_{zz},\sigma_{yy}-\sigma_{zz},\tau_{xy}) + 2k_5\tau_{yz}^2 + 2k_6\tau_{zx}^2}\end{aligned} \tag{8}$$

Since it is difficult to obtain the mechanical properties in out of plane direction, k_5 and k_6 parameters related to the out of plane shear components were adjusted considering the isotropy in out of plane direction. Sener et al. [38, 39] used HomPol4 criterion to define anisotropic behavior of AISI 304 stainless steels. They applied the material model to rectangular cup deep drawing process and could accurately predict the thickness distributions and flange geometry of the formed part.

Within the scope of this study, associated flow rule given in Eq. (9) was adopted to specify the direction of the incremental plastic strain [40].

$$d\varepsilon_{ij}^p = \gamma\frac{df}{d\sigma_{ij}} \tag{9}$$

Here, γ denotes a non-negative multiplier.

Ductile Damage Criteria

In the present work, the generalized plastic work and the modified Mohr-Coulomb (MMC) criteria were used

as basic and advanced damage models, respectively. The theory of these damage models is explained below:

The generalized plastic work criterion

Conventionally, ductile fracture criteria assume that the failure occurs when the integration of a weight function over the plastic strain attains a threshold. It yields,

$$C = \int_0^{\bar{\epsilon}_f} w(\sigma_{ij}) d\epsilon^P \tag{10}$$

Here, w (σ_{ij}) represents a weight function which is also a function of a Cauchy stress tensor. C is a material constant called as damage indicator. In the present work, an energy based ductile damage criterion was used as basic model. This damage model considers the distortional plastic energy stored within the material and assumes that the failure will begin when the distortional energy reaches the critical value [41]. Simple and the expanded form of this criterion are given in Eq. (11).

$$\begin{aligned} C &= \int_0^{\bar{\epsilon}_f} \bar{\sigma} d\bar{\varepsilon}_p \\ &= \int_0^{\bar{\epsilon}_f} (\sigma_{xx} d\varepsilon_{xx} + \sigma_{yy} d\varepsilon_{yy} + \sigma_{zz} d\varepsilon_{zz} + 2(\tau_{xy} d\varepsilon_{xy} + \tau_{yz} d\varepsilon_{yz} + \tau_{zx} d\varepsilon_{zx})) \end{aligned} \tag{11}$$

Here, $\bar{\sigma}$ and $d\bar{\varepsilon}_p$ denote equivalent stress and equivalent plastic strain increment, respectively. Besides, σ_{ij}, τ_{ij} are normal and shear stress components, $d\epsilon_{ij}$ denotes the plastic strain increment components and $\bar{\epsilon}_f$ is the equivalent fracture strain. C_{cr} is referred as critical damage parameter and it is determined by calculating of the area under the equivalent stress – equivalent plastic strain curve of the material. The detailed information about the determination of critical damage parameter will be explained in "Calibration of Ductile Damage Models" section. This ductile damage function was previously applied by Aksen et al. [42] and the successful results were obtained for DP600 steel.

The Modified Mohr-Coulomb (MMC) criterion

Bai and Wierzbicki [43] improved the classical stress-based Mohr-Coulomb criterion and introduced MMC for the spherical coordinate system. This criterion is extensively used in the literature [44–46] and is expressed in Eq. (12).

where, K and n are hardening parameters, b_1, b_2 and b_3 are the parameters related to the fracture behavior of the material. The stress triaxiality (η) and Lode parameter (L) describe the stress state together and are expressed in Eqs. (13) and (14).

$$\eta = \frac{\sigma_1 + \sigma_2 + \sigma_3}{3\bar{\sigma}} \tag{13}$$

$$L = \frac{2\sigma_2 - \sigma_1 - \sigma_3}{\sigma_1 - \sigma_3} \tag{14}$$

Experimental Studies

In the present work, experimental studies are investigated within two groups: Firstly, uniaxial tensile tests (UTTs) were performed to calibrate the yield functions and the generalized plastic work ductile damage criterion, and then HETs were carried out to evaluate the edge stretchability of the materials.

Uniaxial Tensile Test (UTT)

DP steels were considered in this study. These steels are a member of AHSS family, and they become prominent due to their high strength, high formability performance and good weldability properties in the automotive industry. DP steels contain soft ferrite matrix and hard martensitic islands in their microstructures as reported by Alaie et al. [47]. Soft ferrite matrix ensures the ductility, while the hard martensite provides high strength [48]. The difference in hardness between the phases significantly influences the local formability performances, such as edge stretchability or stretch-bending of DP steels, as determined in the study of Heibel et al. [49]. In the present study, DP600 (t_0 = 0.7 mm) and DP800 (t_0 = 1.17 mm) were considered as test materials. UTTs were conducted on an Instron 8872 testing machine with 25 kN capacity. The specimens were cut by laser cutting process along seven orientations (0°, 15°, 30°, 45°, 60°, 75°, and 90°) with respect to the RD. Uniaxial testing machine used in the experiments is shown in Fig. 1.

Tensile tests were repeated three times for each direction and 1×10^{-4} s^{-1} strain rate was applied. Yield stresses and Lankford coefficients of the materials were determined for each direction. ASTM E517-19 [50] standard

$$\bar{\epsilon}_{p,f}(\eta, L) = \left\{ \frac{K}{b_2} \left[b_3 + \frac{\sqrt{3}}{2-\sqrt{3}} (1 - b_3) \left(\sqrt{\frac{3+L^2}{3}} - 1 \right) \right] \left[\sqrt{\frac{1+{b_1}^2}{3+L^2}} + b_1 \left(\eta + \frac{1}{3} \left(\frac{-L}{\sqrt{3+L^2}} \right) \right) \right] \right\}^{-1/n} \tag{12}$$

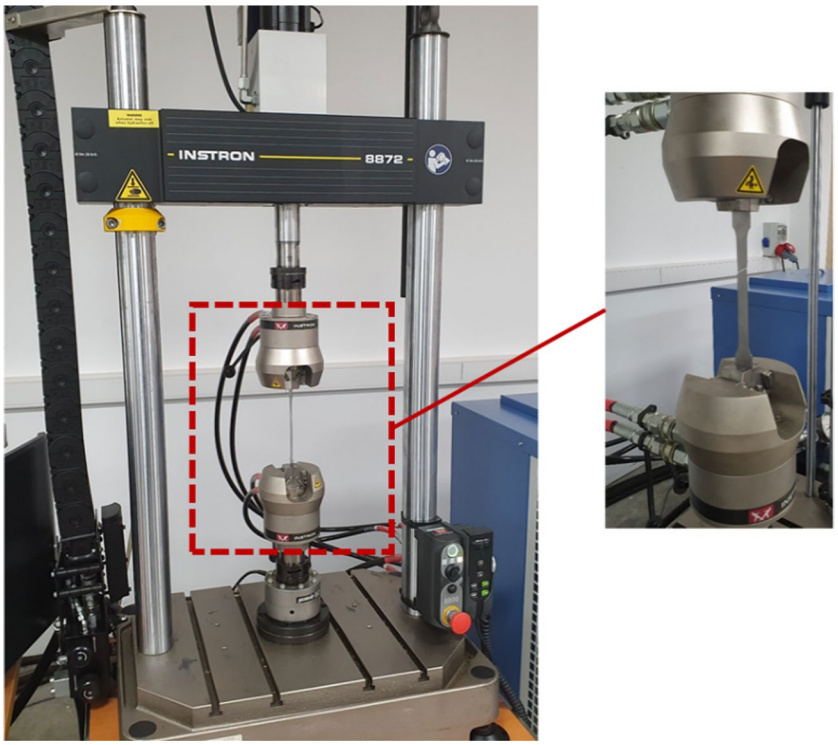

Fig. 1 Tensile test machine

Table 1 Yield stress ratios of the materials in different orientations

Material	$\bar{\sigma}_0$	$\bar{\sigma}_{15}$	$\bar{\sigma}_{30}$	$\bar{\sigma}_{45}$	$\bar{\sigma}_{60}$	$\bar{\sigma}_{75}$	$\bar{\sigma}_{90}$	$\bar{\sigma}_b$
DP600	1.0000	1.0053	0.9565	0.9456	0.9510	0.9324	0.9397	0.8414
DP800	1.0000	1.0013	1.0226	1.0216	1.0266	1.0105	1.0253	1.0140

Table 2 r values of the materials in different orientations

Material	r_0	r_{15}	r_{30}	r_{45}	r_{60}	r_{75}	r_{90}
DP600	0.86	0.85	0.74	0.96	0.76	0.60	1.02
DP800	0.75	0.89	0.98	0.74	0.70	0.85	0.84

was considered in the determination of r values. Yield stress ratios and Lankford coefficients of DP600 and DP800 steels are presented in Tables 1 and 2, respectively. Biaxial yield stresses of the DP600 and DP800 were taken from Stoughton et al. [51] and Cardoso and Moreira [52], respectively.

Flow curve of the materials were defined with Swift isotropic hardening law (Eq. (15)). Experimental data in the RD was taken as reference in the determination of Swift parameters and the hardening parameters were determined by using Levenberg-Marquardt algorithm. Hardening parameters and flow curves of both steels are shown in Table 3 and in Fig. 2, respectively.

$$\sigma_{true} = K(\epsilon_0 + \epsilon_p)^n \tag{15}$$

Table 3 Hardening parameters of the materials

Material	K (MPa)	n	ε_0
DP600	1071	0.1935	0.0110
DP800	1375	0.1754	0.0001

Hole Expansion Test

HETs were performed in compliance with ISO 16,630 standard [53]. Experiments were conducted on a 30-ton hydraulic press. Force and position control of the hydraulic press are provided by using Programmable Logic Controller (PLC). In the experiments, firstly, a hole with 10 mm diameter was punched in the

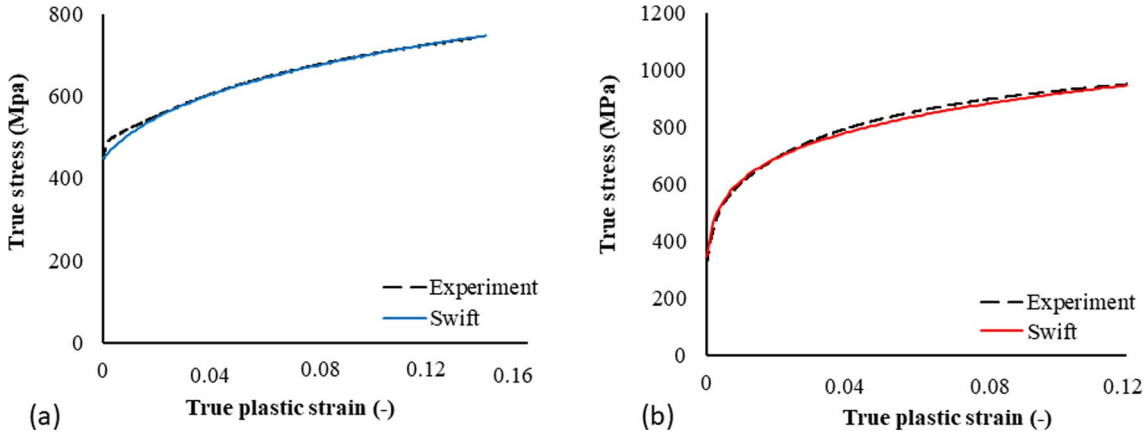

Fig. 2 Flow curves of the materials: **a** DP600; **b** DP800

center of each sheet sample (100 × 100 mm). Numerous factors regarding the hole punching process, such as the cutting speed, alignment of punch and die, the press type, and its stiffness, are simultaneously involved in HET. Levin et al. [54] conducted experiments with different types of presses in different labs and studied the effect of stiffness and coaxiality of tools on HER. From these investigations, they declared that the hole-punching process accounts for 10% of the variability in HER values.

In the present work, a C-frame mechanical press with a 40-ton capacity was used for the hole-punching process (Fig. 3(a)). According to ISO 16,630 standard, 12% of sheet thickness was considered for the clearance and two piercing dies with different diameters were used for DP600 and DP800 to provide the desired clearance due to the different thickness of the materials. After hole piercing process, the holes were expanded with conical punch until a visible crack was observed. Experimental set-up and tool dimensions of HET were shown in Figs. 3(b) and 4.

During the experiments, 21.63 kN and 28.77 kN binder forces were applied to prevent material flow into die cavity for DP600 and DP800, respectively and any lubricant was not applied to the tool and blank interfaces. HETs were repeated five times for each material. When visible cracks through the thickness were observed, the punch movement was stopped (Fig. 5), and the force value was identified with the load cell on the hydraulic press. After performing HETs, the final hole diameters were precisely measured by three-dimensional (3D) scanning method and HERs of the materials were calculated by using the following equation:

$$\mathrm{HER} = \left(\frac{d_1 - d_0}{d_0}\right).100 \tag{16}$$

Where, d_0 and d_1 denote the initial and the final hole diameters, respectively. The determined HERs were

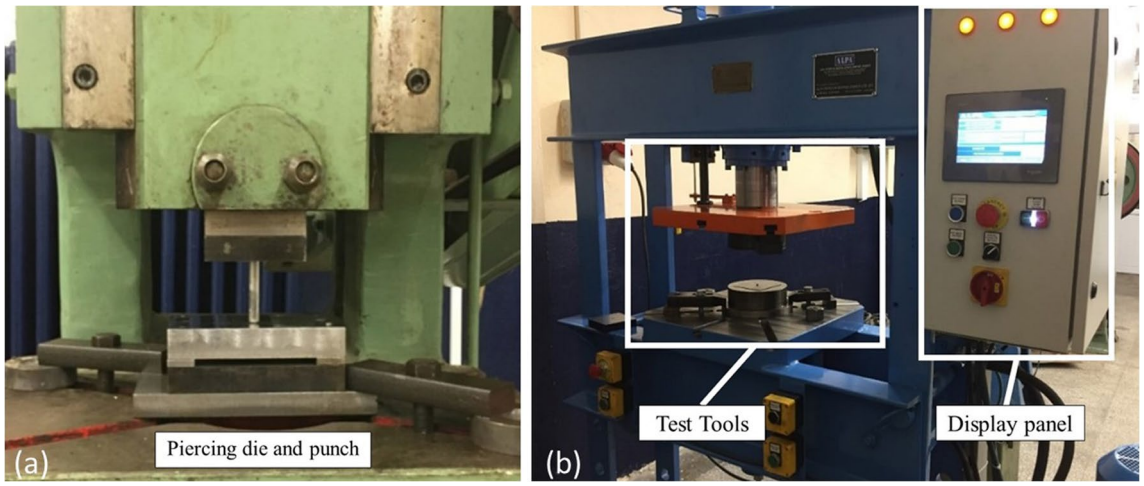

Fig. 3 Experimental set-up **a** Hole punching equipment, **b** HET

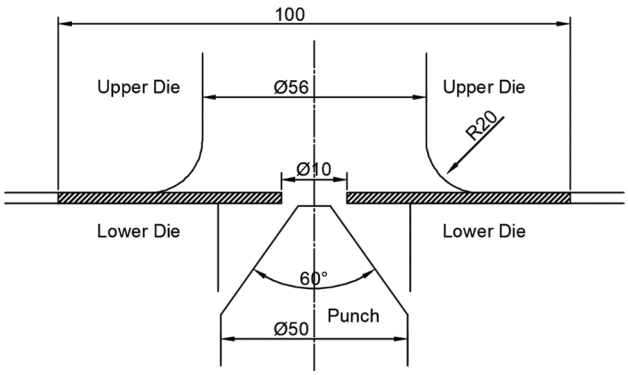

Fig. 4 Dimensions of the test tools

compared to evaluate the edge stretchability of the materials. HER values of the samples were calculated as 70.9% and 50.9% for DP600 and DP800 steels, respectively. From these comparisons, it was shown that DP600 exhibited higher edge formability than DP800.

Determination of Constitutive Model Parameters

In this section, the constitutive model parameters were calculated. Initially, the coefficients of the anisotropic stress potentials, then the parameters of the ductile fracture models were calibrated.

Calibration of Anisotropic Stress Potentials

Firstly, anisotropic stress potentials were calibrated with UTT data and then their prediction capabilities were evaluated. The coefficients of Hill48 and HomPol4 yield functions were determined by applying the identification methods explained in "Hill48 stress potential" and "The fourth-order homogeneous polynomial stress potential" sections, respectively. Four experimental data (r_0, r_{45}, r_{90}, σ_0) for Hill48, eleven experimental data (σ_0, σ_{15}, σ_{45}, σ_{75}, σ_{90}, σ_b, r_0, r_{15}, r_{45}, r_{75}, r_{90}) for HomPol4 were used. The coefficients of Hill48 and HomPol4 stress potentials for DP600 and DP800 are shown in Tables 4 and 5, respectively.

The planar variations of the plastic properties (yield stress ratio and Lankford coefficient) were determined according to these functions by using yield condition and normality rule in plasticity theory. The calculated results were compared with experiments to evaluate the stress potentials. The comparison results for DP600 and DP800 are shown Figs. 6 and 7, respectively.

It is seen from the Fig. 6 that HomPol4 yield function could simultaneously predict stress ratio and r-value variations, while Hill48 criterion could only predict r-value anisotropy. As for DP800, a different result was observed. HomPol4 showed oscillations in the predictions of the angular variations of the stress ratios and the predictions of the model were worse than Hill48 at interval angles in contrast to the angular variations of the r-values. Although Hill48 parameters were defined with r values, accurate description of stress anisotropy by the criterion was completely coincidental. DP800 exhibited weak stress anisotropy, therefore Hill48 could capture the stress variations in the sheet plane. As the second stage in the evaluation of the anisotropic stress potentials, yield locus contours were taken into account, and they were compared with experimental stress ratios for both of the materials. Figure 8(a) and (b) show the comparisons of the predicted yield locus contours from Hill48 and HomPol4 functions with experimental data for DP600 and DP800, respectively.

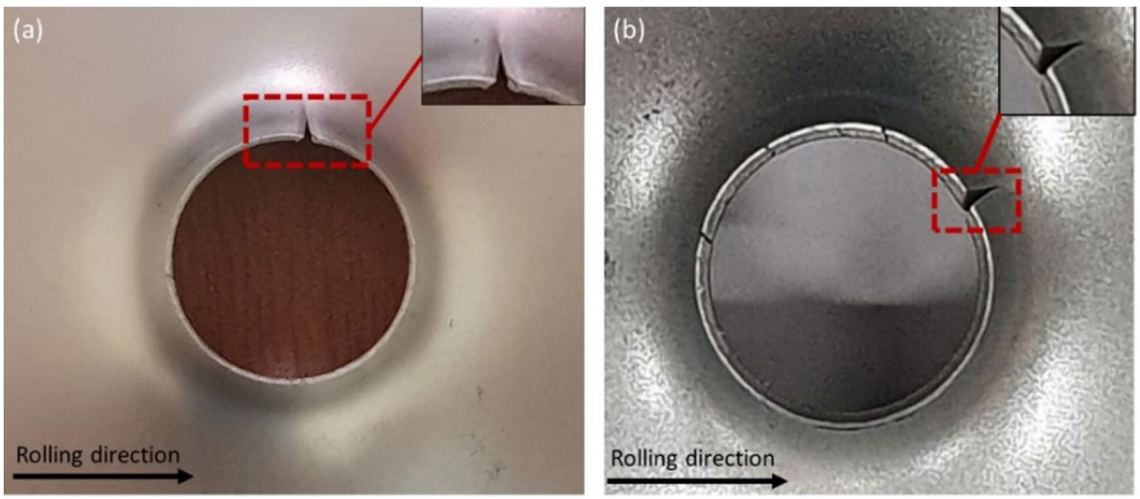

Fig. 5 Samples after HETs: **a** DP600; **b** DP800

Table 4 Hill48 coefficients

Material	F	G	H	L	M	N
DP600	0.453	0.538	0.462	1.5	1.5	1.447
DP800	0.510	0.571	0.429	1.5	1.5	1.341

Table 5 HomPol4 coefficients

Material	a_1	a_2	a_3	a_4	a_5	a_6	a_7	a_8	a_9
DP600	1.000	-1.849	4.152	-2.590	1.282	6.499	-7.663	7.386	11.798
DP800	1.000	-1.714	2.408	-1.653	0.905	9.258	-5.436	2.728	7.193

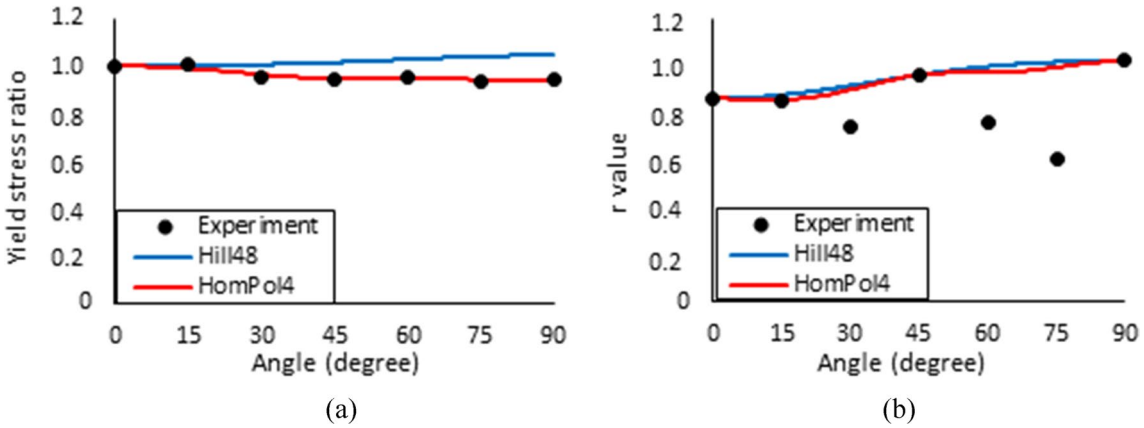

Fig. 6 Angular variations of plastic properties for DP600 **a** yield stress ratio, **b** r value

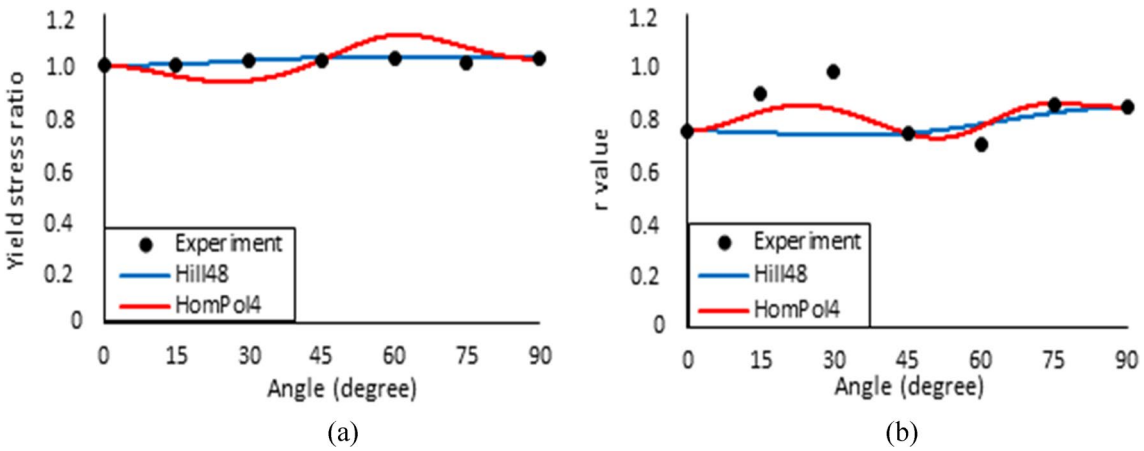

Fig. 7 Angular variations of plastic properties for DP800 **a** yield stress ratio, **b** r value

It is seen from Fig. 8 that both uniaxial and biaxial yield stress ratios could accurately be predicted by HomPol4 yield criterion, whereas Hill48 couldn't predict the uniaxial stress ratio along TD and biaxial stress ratio of DP600 as well as the biaxial stress ratio of DP800. These results are related to the inputs used in the coefficient identification of the stress potentials. Hill48 stress function is calibrated with only r-values, while HomPol4 criterion accepts both stress ratio and r-values as input. Therefore, HomPol4 criterion could describe the planar anisotropy of the materials more accurately than Hill48 criterion.

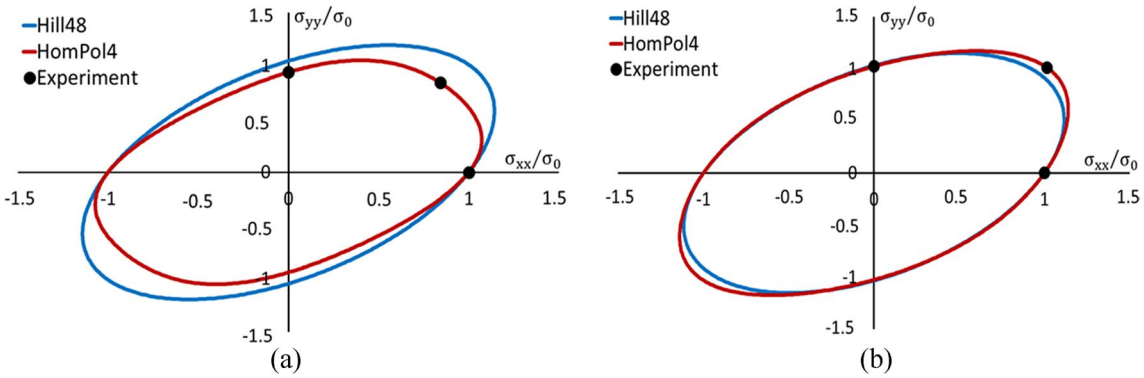

Fig. 8 Yield loci contours: **a** DP600; **b** DP800

Table 6 The sizes and number of elements used in FE models

	Element size in gauge length (mm)	Number of elements through thickness
Case 1	1.00×1.00	2
Case 2	0.50×0.50	4
Case 3	0.25×0.25	8

Calibration of Ductile Damage Models

In this section, the parameters of the ductile damage models were calibrated: Firstly, the generalized plastic work and then MMC criteria were calibrated. Before the ductile damage models are calibrated, a mesh independence study was carried out to determine an optimum element size in terms of both accuracy and computation time. Therefore, three different quarter FE models of UTT were created with eight node hexahedral fully integrated solid elements. In the mesh sensitivity study, the gauge length was discretized with different mesh sizes and the number of elements through the thickness direction of the specimen was varied. Element sizes used in mesh sensitivity study are given in Table 6.

After definition of the numerical parameters, FE analyses for each case were carried out in Marc software and Case 2 was selected. HomPol4 yield function was used in the mesh sensitivity analyses. After the determination of the optimum mesh size, critical damage parameter (C_{cr}) of the generalized plastic work criterion was calculated for both materials. As mentioned in the "The generalized plastic work criterion" section, C_{cr} is determined by calculating of the area under the flow curve up to fracture strain. However, it is mentioned that classical transformation equations, which determines the relationship between engineering and true stress vs. strain data, are valid up to the peak point due to the initiation of tri-axial stress state [55]. Beyond the necking point, the true stress-strain curve can be obtained by inverse method. Therefore, flow curves of the materials were inversely identified by replicating the experimental force-displacement curves in this study. Figure 9(a) and (b) show that force-displacement responses of the FE analyses agree well with the experimental curves without any correction.

Equivalent stress-equivalent strain curves were acquired from FE analyses and the area of the curves up to equivalent fracture strain were calculated by using trapezoidal rule. The values of C_{cr} for two materials are given in Table 7.

The values of C_{cr} were separately determined according to yield functions. However, only the damage parameters obtained from HomPol4 yield criterion were considered due to the small differences between the predicted force-displacement curves.

After calibration of the generalized plastic work criterion, the MMC model was calibrated. The required experimental data for the calibration of DP600 and DP800 were taken from the studies performed by Qin and Beese [56] and Kusche et al. [57], respectively. The model parameters were determined and their values for both materials were given in Table 8. After the determination of the parameters, the fracture locus of the calibrated MMC model was obtained and compared with the experimental data, as shown in Fig. 10.

The results obtained for DP600 steel were acquired from the central hole tension, butterfly, punch, and notched (over width notches with the radius values of 6.67 mm, 10 mm, and 20 mm) tensile test specimens, which represent different stress states. Among these specimens, central hole tension and punch specimens represent the uniaxial tension ($\eta = 0.33$) and balanced biaxial tension lines ($\eta = 0.66$), respectively. The notched specimens cover the range from uniaxial tension ($\eta = 0.33$) and plane strain tension ($\eta = 0.58$) lines. The different combinations of horizontal and vertical forces were applied to the butterfly specimen. Thereby, pure shear ($\eta = 0$) and plane strain tension ($\eta = 0.58$) stress states were characterized [56]. As shown in Fig. 10, experimental data corresponding to the uniaxial, plane strain and the balanced biaxial tension were considered for

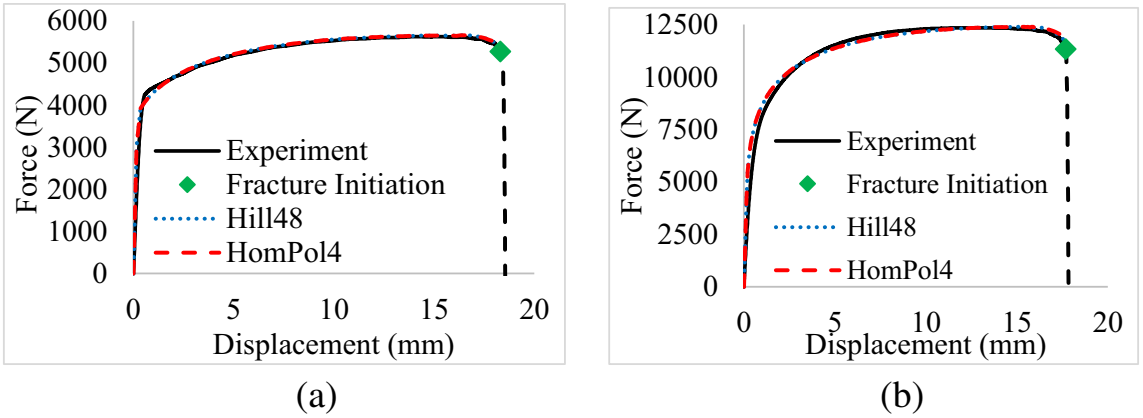

Fig. 9 Comparison of numerical and experimental force-displacement curves: **a** DP600; **b** DP800

Table 7 Critical damage parameters for DP600 and DP800

Materials	C_{cr}
DP600	426.900
DP800	497.569

the calibration of DP600 due to the variation of stress state between uniaxial and plane strain along the width of the sample in conical HET [56]. For DP800, plane strain (notched over thickness), notched (over width) tensile test, and standard tensile test specimens were utilized, and two notched tensile test specimens referred to as DB-20 (20 mm notch radius) and DB-50 (50 mm notch radius) in the study [57] were utilized in the calibration due to the observation of the scatter experimental points at the high-stress triaxiality region. In addition, 2D fracture loci, 3D fracture loci were also constructed and demonstrated in Fig. 11 for both materials.

Application Study

Table 8 MMC ductile fracture model parameters

Materials	b_1	b_2	b_3
DP600	0.07	519	0.950
DP800	0.01	622	0.902

The developed constitutive model was implemented into implicit FE code Marc via developed material subroutine HYPELA2. The model was firstly applied to uniaxial tensile and then hole expansion tests to predict fracture. In order to predict fracture initiation with the generalized plastic work ductile damage model, energy value and damage percentage for each integration point were calculated throughout the analysis by using Eqs. (10) and (17), respectively. When the damage percentage of an element reaches 100%, fracture initiates in the FE model [58].

$$\%\ \text{Failure} = \left(\frac{\text{Energy value}}{\text{Critical damage parameter}}\right) \times 100 \qquad (17)$$

The computation steps related to the prediction of damage are shown in the flow chart given in Fig. 12 and the obtained results are explained below:

Application to Uniaxial Tensile Test (UTT)

The developed model was firstly applied to UTT to predict fracture initiation. In order to evaluate the effect of anisotropic yield functions on the fracture prediction, the variations of the equivalent plastic strains predicted from the yield functions during the deformation were obtained and the equivalent fracture strains were determined for each yield function, because the displacement to the fracture is known from the tensile test. Investigation was conducted at the center of the specimen. Figure 13(a) and (b) show the variation of the equivalent plastic strain with displacement for DP600 and DP800, respectively.

It is seen from Fig. 13(a) and (b) that both yield functions predicted the onset of diffuse necking at the same displacement values and small differences between the equivalent fracture strains predicted from the yield criteria were observed. Besides, the variation rate of the equivalent plastic strain consistently increased after the diffuse necking point due to occurrence of non-uniform strain distribution. Plastic work distributions were investigated, and failure locations were evaluated according to the stress potentials. Figures 14 and 15 show the plastic work distributions predicted from the material models for DP600 and DP800, respectively.

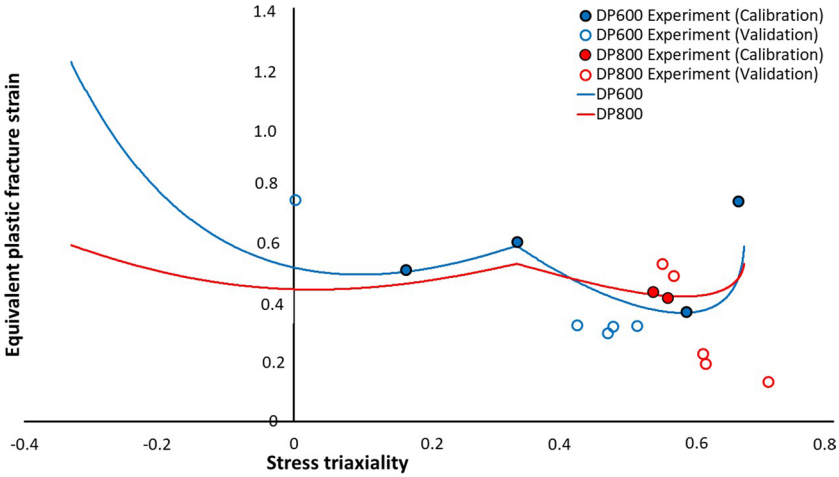

Fig. 10 Comparison of the calibrated MMC fracture locus with experimental data

As it is seen from Figs. 14 and 15 that the predicted plastic work distributions from both yield functions were concentrated at the center of the specimen and failure was predicted at the same location.

Application to Hole Expansion Test (HET)

FE model of HET was prepared in Marc FE program. Due to symmetry, only quarter model was created. Tools were considered as rigid and the blank was discretized with fully integrated eight-node solid elements known as Hex7 in Marc 2018 Volume A and Volume B [59, 60]. Four elements were used along the thickness direction in the model. Blank was divided into two regions and element density was increased at the hole edge to predict strains precisely. The in-plane mesh size was taken as 0.5 mm x 0.27 mm and 32 elements were used along the circumferential direction at the hole edge. A similar mesh structure to that in tensile test (Case 2) was created in FE model of HET. Global X direction was defined as RD in the model and friction coefficient between the surfaces was assumed as 0.1 which was recommend from Choi et al. [61]. FE model of the HET and the mesh layout of the blank are demonstrated in Fig. 16(a) and (b), respectively.

FE analyses of HET were performed for both yield function and firstly the fracture displacements were predicted. The fracture displacements were extracted from simulation at the moment when the damage percentage value of the critical element reached one hundred (Fig. 17(a) and (b)). Then the predicted fracture displacement values were compared with experimental values for both materials (Fig. 18).

It is seen from Fig. 18 that the predicted fracture displacements from the models were compatible with the experimental data for both materials. This result showed that damage model was accurately calibrated. When the predictions of the yield criteria were investigated, small differences (about %3) were observed between Hill48 and HomPol4 predictions for both of the materials. However, anisotropic yield functions

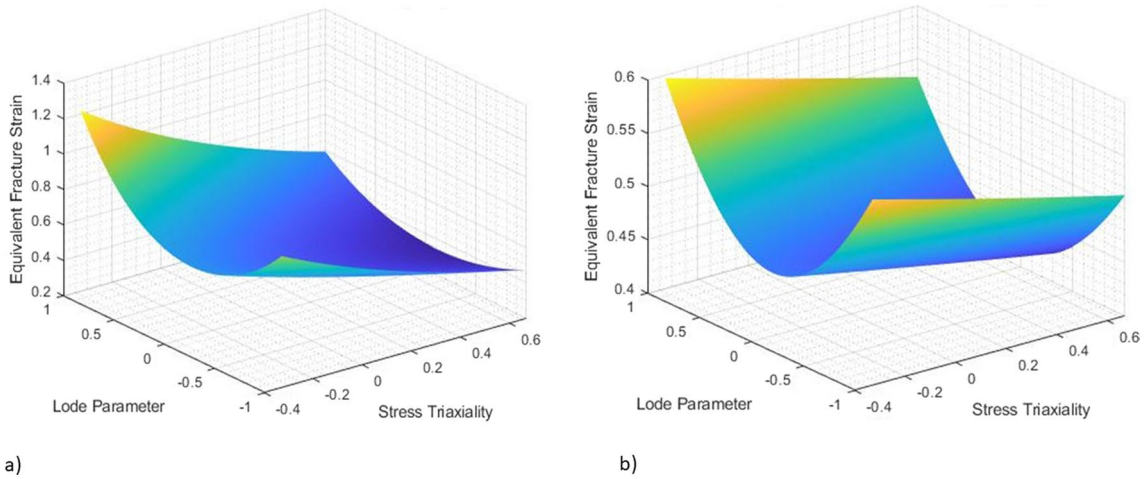

Fig. 11 3D Fracture loci for **a** DP600, **b** DP800

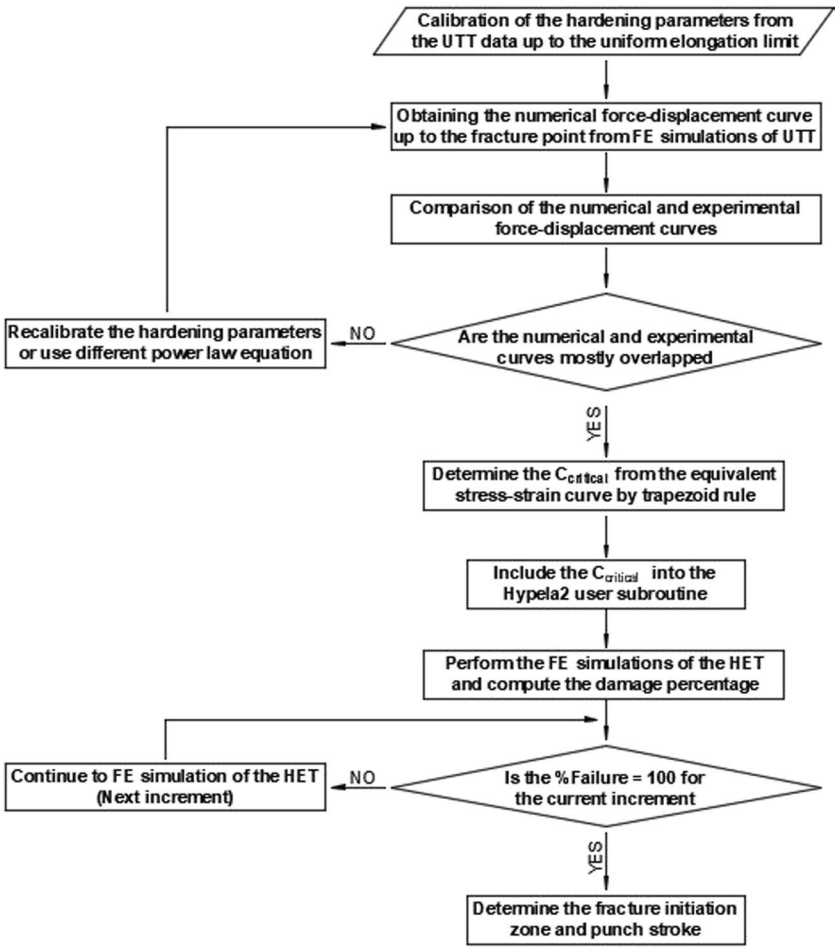

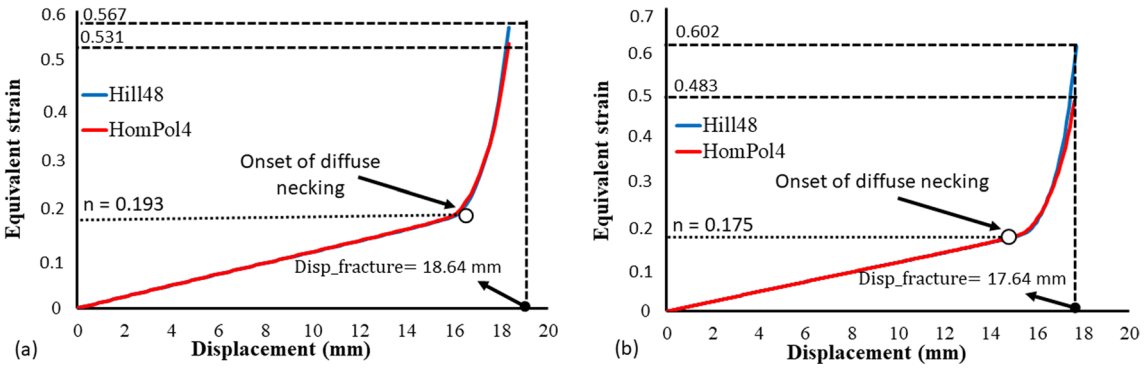

Fig. 13 Evolution of equivalent plastic strain with displacement: **a** DP600; **b** DP800

aren't evaluated according to only fracture displacement predictions, investigation of the HER values and fracture location predictions are also required. Therefore, these outputs were taken into consideration and the predictions were compared with experimental results in the second phase of the work. In order to accurately examine the effect of yield functions, the numerical and experimental comparisons were performed at same punch displacement values which edge fracture is observed in the experiments. Figure 19 shows the predicted and experimental HER values at the fracture displacements of DP600 and DP800.

It is seen from the comparisons that the numerical HER values were slightly higher than experimental values for both materials and small differences were observed between the predictions of the anisotropic stress functions. For DP600, Hill48 and HomPol4 models predicted HER with only 1.64%

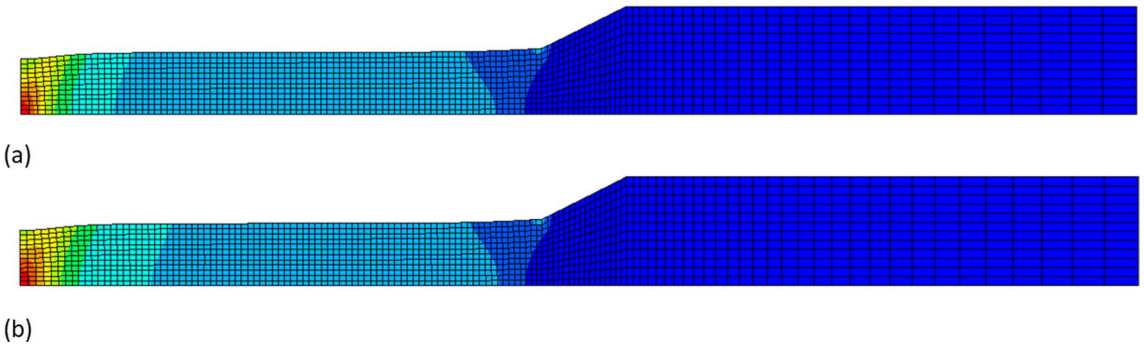

Fig. 14 Plastic work distributions of DP600: **a** Hill48; **b** HomPol4

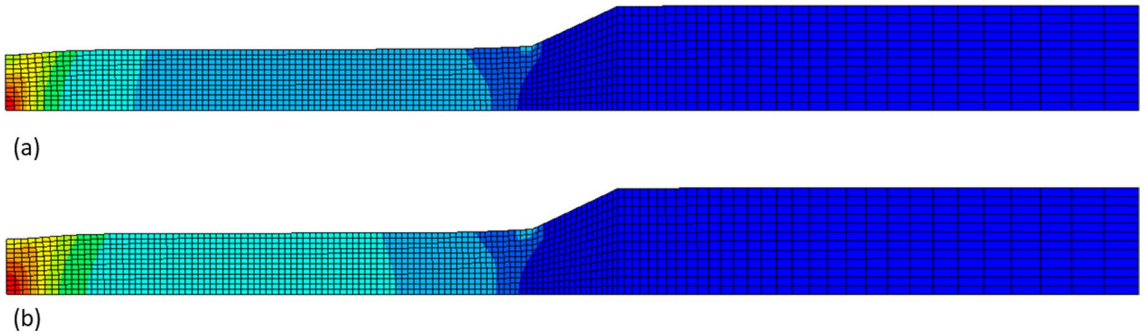

Fig. 15 Plastic work distributions of DP800: **a** Hill48; **b** HomPol4

and 0.31% errors. While for DP800, these anisotropic functions predicted with 9.51% and 9.9% errors, respectively. As the third criterion, fracture locations on the samples were considered to investigate the influence of anisotropy. The angles between the cracks and RD of the samples were measured by using 3D scanning method and fracture locations were determined experimentally. Then, these locations were compared with FE results. Plastic work distributions along the hole edge were taken into consideration in the numerical results. Figures 20 and 21 show the comparisons of the numerical and experimental crack locations for DP600 and DP800, respectively.

Figures 20 and 21 show that HomPol4 yield function predicted quite well fracture locations of the materials. Accurate description of in-plane anisotropy has effect on the prediction of the fracture location. According to Hill48 criterion, stress ratios and r-values of DP600 increased monotonically from RD to TD (Fig. 6). However, in the experimental results, stress ratios of the material decreased along the mentioned direction and oscillations were observed in its r-values. This behavior could well be represented by HomPol4 yield criterion and thus the model could more accurately predict the fracture location at the hole edge. As for DP800, this material showed weak stress anisotropy as mentioned previously, while it exhibited strong r-values anisotropy (Fig. 7). Therefore, it can be said that the planar distributions of the r-values could play more dominant role in the prediction of fracture location. R values of the material especially at interval angles could more accurately predicted with HomPol4 criterion and therefore the crack orientation was predicted from the criterion is more compatible with the experiment.

Comparison with MMC criterion

The studies performed by Bao and Wierzbicki [62] and Lou et al. [63] showed that equivalent plastic strain value at fracture depends on the stress triaxiality and Lode parameter. In order to investigate the effect of these parameters on the predictions, the MMC criterion was implemented into Hypela2, and FE simulations of the conical HET were performed with HomPol4 anisotropic model. Fracture displacements and fracture location predictions of both damage models were compared with each other, and experiments as shown in Figs. 22, 23 and 24.

It is seen from Fig. 22 that the numerical results predicted from the MMC model showed better agreement with the experimental results. The error in the predictions decreased from 9.34 to 3.30% for DP600 and from 7.19 to 0.72% for DP800 compared to the generalized plastic work criterion. In this regard, the MMC criterion showed and enhancement in punch stroke prediction over the plastic work criterion. As

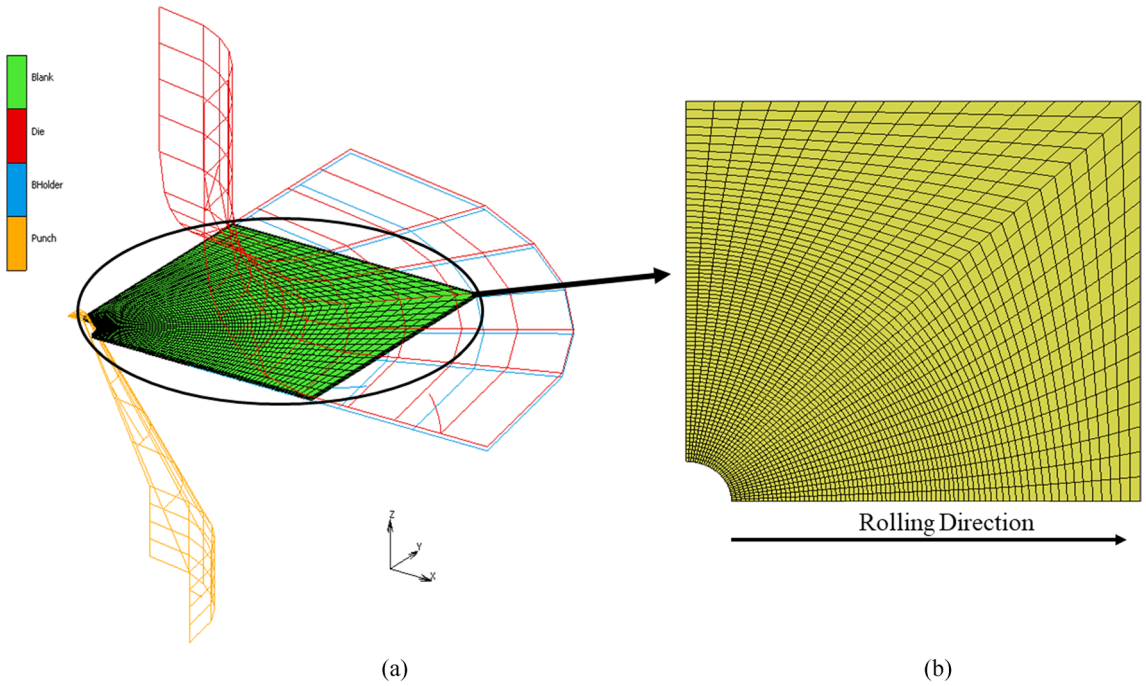

Fig. 16 **a** FE model of HET; **b** mesh layout

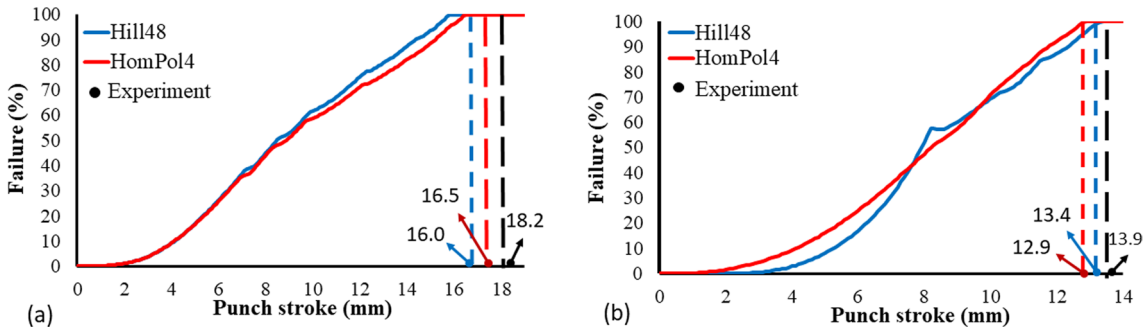

Fig. 17 The variation of the damage percentage with punch stroke: **a** DP600; **b** DP800

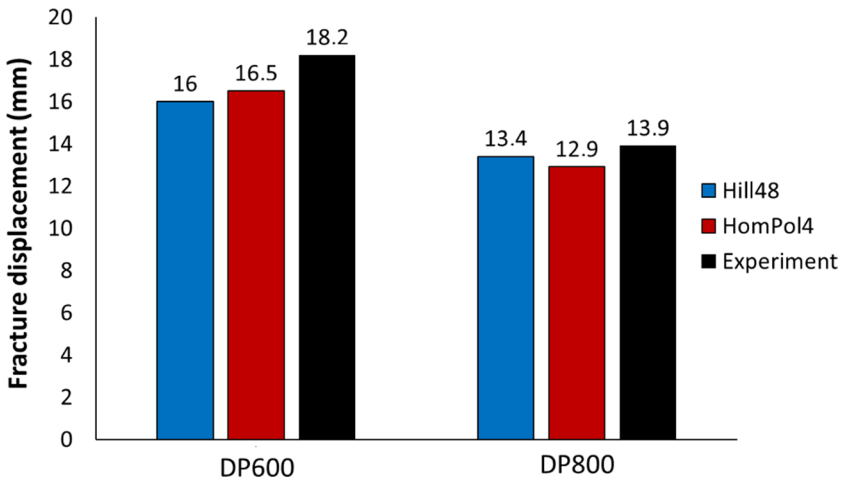

Fig. 18 The numerical and experimental fracture displacement values

for the fracture location predictions, it is seen from Figs. 23 and 24 that both models predicted the edge fracture in the same location for DP600 and DP800. This result shows that the prediction of fracture location is directly associated with the prediction capability of the anisotropic stress potential.

Effect of out-of-plane anisotropy

In the present work, the effect of the out-of-plane anisotropy on fracture predictions was also investigated. In order to investigate this effect, two different cases were considered for the Hill48 criterion (L = M = 2 and L = M = 1), and FE analyses of conical HET were performed for each case. HER values at the experimental fracture displacements and the fracture locations for both materials were predicted and compared, as shown in Figs. 25, 26, and 27.

As it is seen from Fig. 25 that, the predicted HER value decreases with the increase of *M* and *N* for both DP steels. However, the amount of decrease in HER value was not significant. When the predictions of the fracture location are

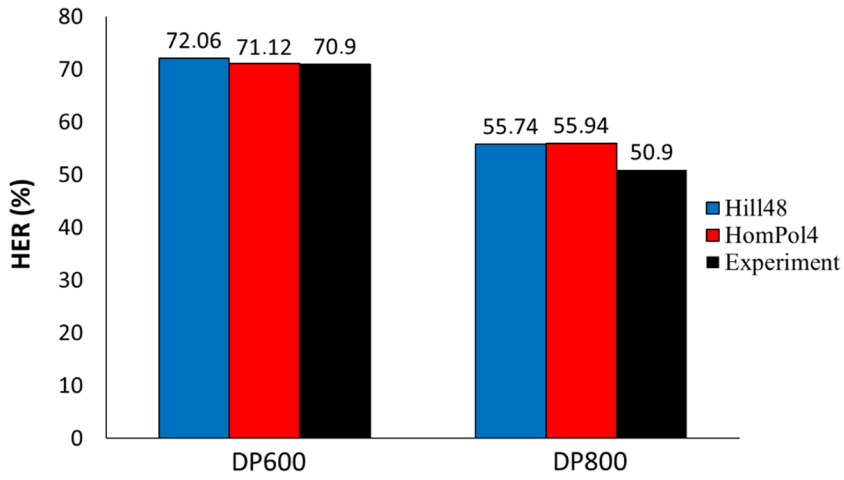

Fig. 19 The numerical and experimental HER values

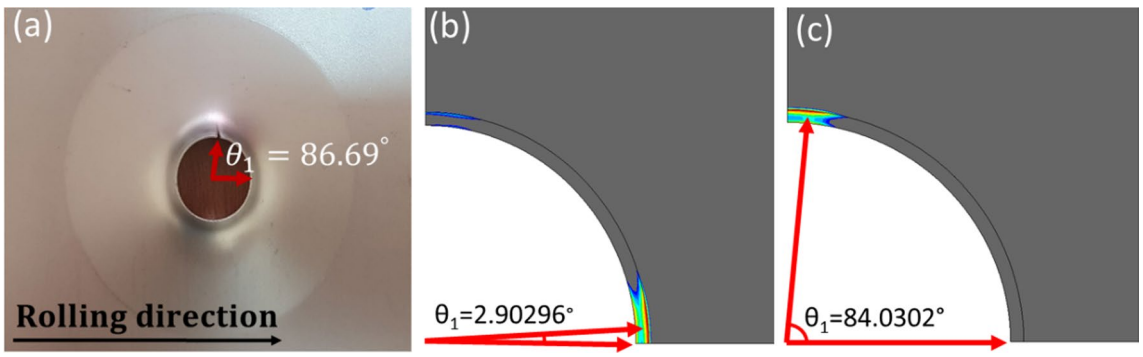

Fig. 20 Experimental and numerical fracture locations of DP600: **a** Experiment; **b** Hill48; **c** HomPol4

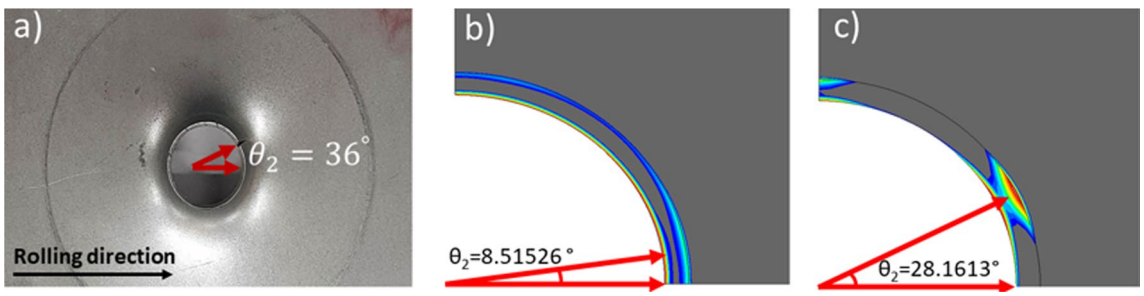

Fig. 21 Experimental and numerical fracture locations of DP800: **a** Experiment; **b** Hill48; **c** HomPol4

investigated, it is seen that the failure was predicted at the same location for all coefficients. In this regard, the out-of-plane anisotropy has a negligible effect on predicting the fracture initiation location.

Variation of Stress-Triaxiality at the Hole Edge

In order to investigate the stress state and to also determine fracture mode, the variation of stress-triaxiality at the hole edge during deformation was evaluated. Stress-triaxiality is a significant parameter which has effect on the fracture strain of the material, and it can be described as the ratio of the hydrostatic stress (σ_h) to the equivalent stress $(\overline{\sigma})$ [64]. The value of this parameter changes based on the loading type, and it is equal to 1/3 under uniaxial tension. Figure 28 shows the evolution of the stress-triaxiality with equivalent strain during UTT and HETs. Two nodes, which one of them is from center of specimen for UTT and the other is from the outer edge of the hole for HET, were selected and the evolutions of the stress-triaxiality with equivalent strain were obtained both materials.

It is seen from Fig. 28 that stress-triaxiality in UTT reached immediately to 0.33, however it could converge to the same value after a certain deformation in HET. It can be said from this result that the deformation behavior in the outer region of the hole is close to the UTT conditions, but hole edge is subjected to larger deformations than UTT. This additional deformation could be attributed to the compatibility between the hole edge and its adjacent region. Similar results were also obtained by Lee et al. [23], Chung et al. [26] and Paul [65].

Conclusions

The main purpose of this study is to exhibit failure prediction capability of polynomial-based yield functions with a basic and an advanced ductile damage models. In the present work, a constitutive model considering material anisotropy and ductile fracture was developed and the effect of anisotropy on fracture prediction was investigated. The proposed model consists of an anisotropic yield function and a ductile fracture criterion. The model was applied firstly to uniaxial

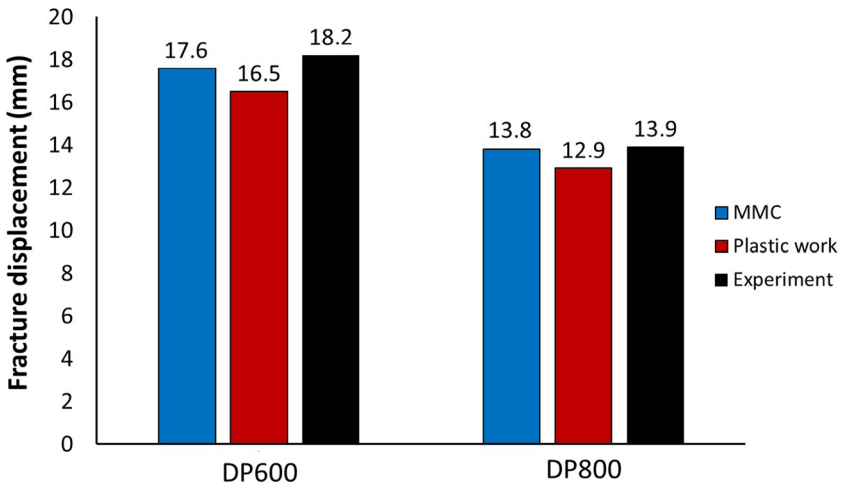

Fig. 22 Comparison of the predicted and experimental fracture displacements

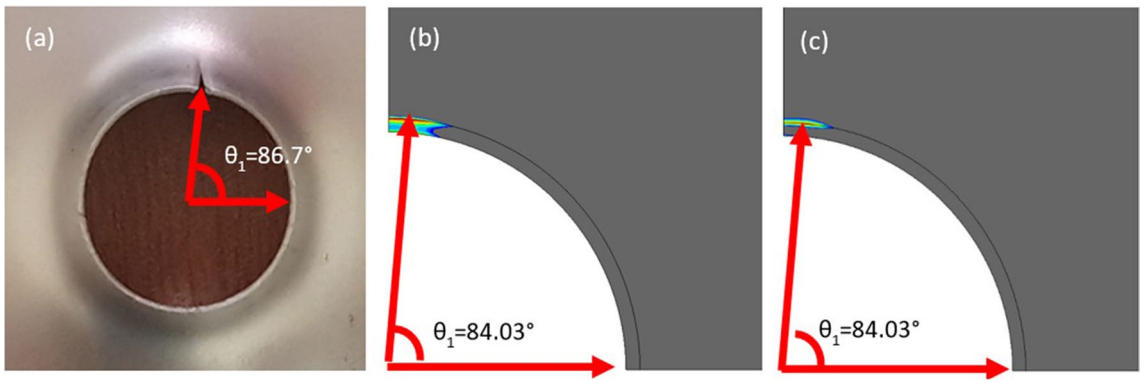

Fig. 23 Experimental and numerical fracture locations of DP600: **a** Experiment, **b** Plastic work, **c** MMC

tensile tests (UTT) and then to hole expansion tests (HET) of dual phase steel sheets for validation. The study was conducted as two stages: In the first stage, quadratic Hill48 and non-quadratic HomPol4 criteria were used in conjunction with generalized plastic work ductile fracture criterion as basic damage model in order to investigate the effect of anisotropy on the fracture prediction. In the second stage, the MMC criterion was considered as advanced damage model to investigate the effect of stress triaxiality and Lode parameters on the predictions. Stroke values at fracture, hole expansion ratios (HER), and fracture locations on the samples were predicted by these models and the numerical results were compared with the experiments. Based on the obtained results, the following conclusions could be drawn:

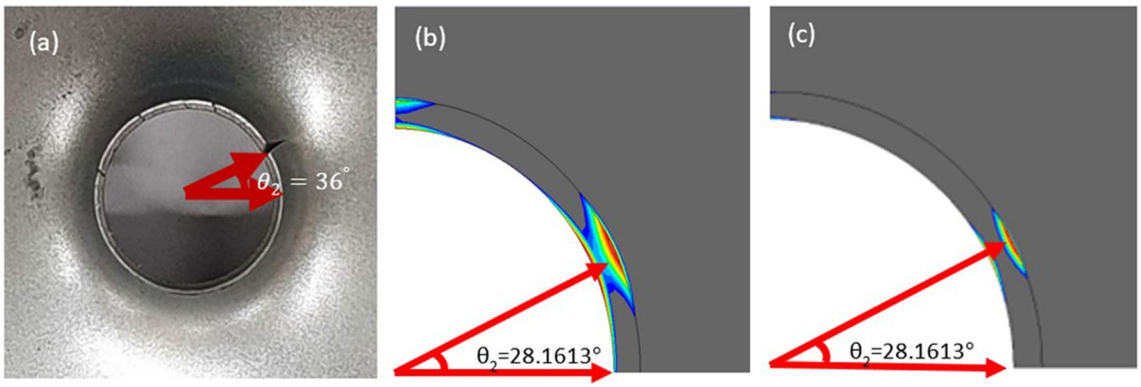

Fig. 24 Experimental and numerical fracture locations of DP800: **a** Experiment, **b** Plastic work, **c** MMC

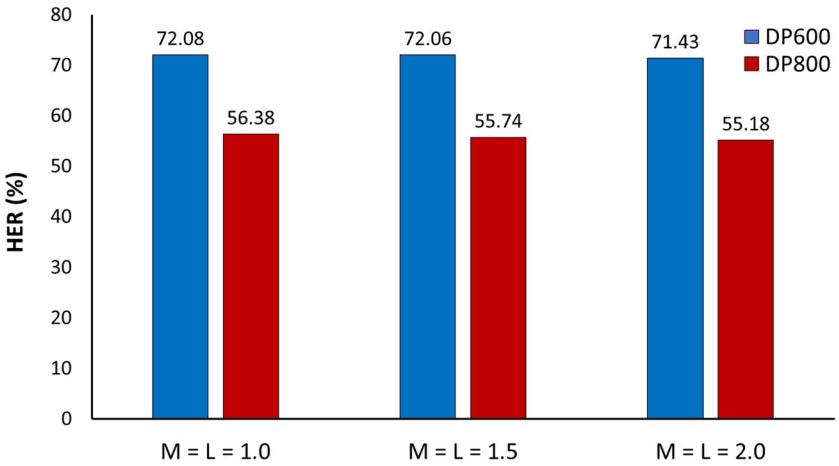

Fig. 25 The predictions of HER values in the different out-of-plane anisotropy coefficients

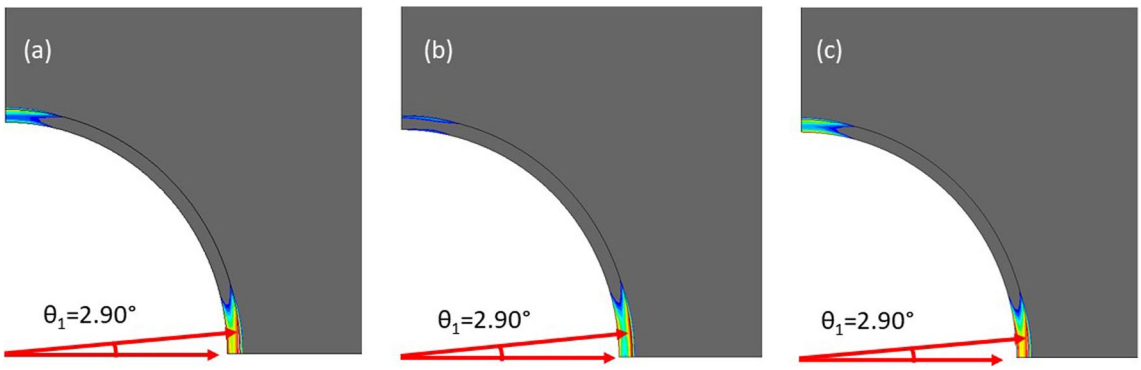

Fig. 26 The numerical fracture locations of DP600: **a** L = M = 1, **b** L = M = 1.5, **c** L = M = 2

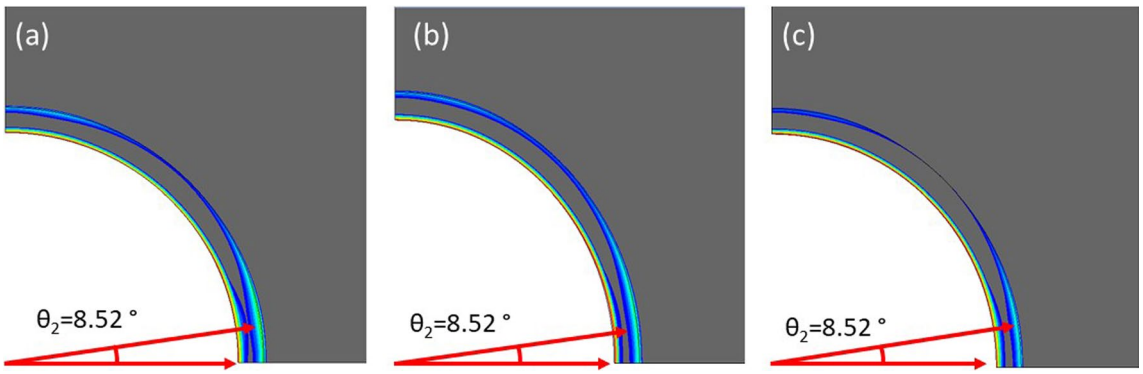

Fig. 27 The numerical fracture locations of DP800: **a** L = M = 1, **b** L = M = 1.5, **c** L = M = 2

a) High difference between engineering fracture strains in UTT and HER values was observed for both DP600 and DP800. This indicates that strain localization and plastic instability are delayed at the hole edge, although it deforms uniaxial tension mode. In addition to that the variation of the stress-triaxiality at the outer region of the hole edge also confirmed this result because it reached to 1/3 at higher strain level than that of UTT.
b) When the predicted fracture displacements, HER values and fracture locations were investigated, no significant differences were observed between the anisotropic stress potentials in the predictions of fracture displacement and HER values, while crack locations were predicted in different angles by the models. HomPol4 yield criterion could accurately predict the crack orientation for both DP600 and DP800. This result could be associated with the description of the in-plane anisotropy. HomPol4 model could reproduce the planar anisotropy of the materials more accurately than Hill48 criterion. Therefore, the predicted crack locations by Hill48 model couldn't satisfy with the experiments.
c) Even if the generalized plastic work criterion is a practical method in terms of calibration process, this criterion may lead to inaccurate results for the materials exhibiting significant instability. However, it can ensure precise results for the materials showing limited amount of strain localization. Although the HomPol4 yield criterion in conjunction with the plastic work criterion could provide a compatible prediction of the crack initiation locations for both steels, the implemented theoretical model with the generalized plastic work criterion could not predict the fracture stroke. When the MMC criterion was included in the material model, the HomPol4 criterion could better predict the fracture initiation stroke in HET. Therefore, by involving the stress triaxiality and Lode parameter in the ductile fracture model, fracture initiation strain can be better predicted for the widespread stamping operations.
d) When the differences between the predictions of the generalized plastic work and MMC ductile fracture criteria were investigated, significant enhancements in the fracture displacement predictions were observed due to the inclu-

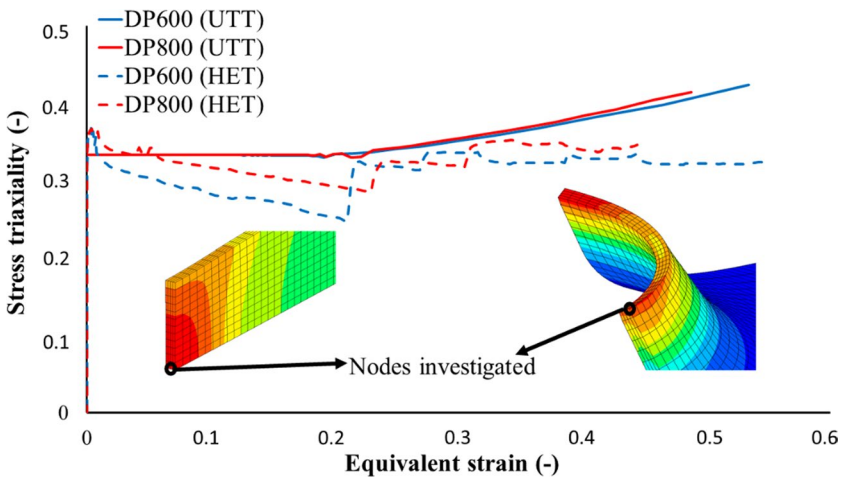

Fig. 28 Evolution of stress-triaxiality during UTT and HETs for DP600 and DP800

sion of the stress triaxiality and Lode parameters. However, fracture initiation location predictions of both criteria were the same. This result showed the importance of the anisotropic stress potential used in the constitutive model.

e) It is seen from the FE simulations performed with different out-of-plane anisotropy coefficients that the out-of-plane anisotropy has no significant effect on the fracture predictions in conical punch configuration of HET. The effect of out-of-plane stresses was also discussed in the study of Lee et al. [23], and the out-of-plane stress effect is found to be negligible in HET. The reason is that the out-of-plane stress was observed to be much lower than the in-plane stresses. In the current study, the maximum out-of-plane stresses were predicted as %4.7 and %10.8 of the in-plane stress values for DP600 and DP800 steels, respectively. Since the out-of-plane stresses have no dramatic effect, the out-of-plane anisotropy could not influence the results notable as well in HET. On the other hand, the effect of out-of-plane anisotropy and stress may be significant for different stamping operations, such as the Nakajima test and the cup drawing process. Bettaieb and Meraim [66] stated that the out-of-plane compressive stresses could postpone the early localization and increase the failure strain in FLC prediction. Besides, Liu et al. [67] pointed out that incorporating the out-of-plane anisotropy increased the prediction capability in the cup drawing process.

f) It was observed that, with a precisely defined yield locus, the damage prediction capability of the generalized plastic work criterion was significantly increased. It was also concluded that a proper yield locus definition is required to determine the failure initiation location accurately.

g) HomPol4 yield criterion is an effective potential to predict the failure locations even with a basic damage model. It predicts the crack initiation near the TD for DP600 and between RD and DD for DP800, which are compatible with the experimental crack locations. The crack location of DP600 was precisely captured, but there was a minor discrepancy for the DP800 steel. Adopting the yield criteria having higher anisotropy parameters, such as HomPol6, Cazacu2018 [68], may provide better r-value representation and can increase the prediction performance; accordingly, the crack initiation location for DP800 steel may be captured more accurately. For the cases in which the crack initiates between RD and DD or DD and TD, the yield criteria having higher number of parameters, which make it possible to capture the plastic properties in intermediate orientations, may provide better correlations.

Acknowledgements This work has been supported by Yildiz Technical University Scientific Research Projects Coordination Unit under project number FBA-2019-3721. The authors would like to thank Yildiz Technical University Scientific Research Projects Coordination Unit for financial support.

CRediT Authorship Contribution Statement Conceptualization [Mehmet Fırat]; Project administration [Mehmet Firat]; Formal analysis and investigation [Toros Arda Akşen, Bora Şener]; Methodology [Mehmet Fırat], [Emre Esener]; Software [Toros Arda Akşen], [Mehmet Firat]; Validation [Toros Arda Akşen], [Bora Şener]; Visualization [Emre Esener], [Bora Şener]; Writing-original draft preparation [Toros Arda Akşen], [Bora Şener]; Writing-review & editing [Emre Esener], [Mehmet Firat]; Supervision [Mehmet Firat].

Data Availability Data available on request from the authors.

Declarations

Competing Interest The authors declare that they have no relevant financial or non-financial interests to disclose.

References

1. Chen XM, McKune PM, Prince DG (2003) Automotive applications of stretch flange high strength steel. SAE Tech Pap Ser 2003–01–0690. https://doi.org/10.4271/2003-01-0690
2. Hance BM (2017) Practical application of the hole expansion test. SAE Int J Engines. https://doi.org/10.4271/2017-01-0306
3. Paul SK (2019) Effect of punch geometry on hole expansion ratio. Proc Inst Mech Eng Part B: J Eng Manuf. https://doi.org/10.1177/0954405419863222
4. Sadagopan S, Urban D, Wong C, Huang M, Yan B (2003) Formability characterization of a new generation of high strength steels. Tech Rep. https://doi.org/10.2172/1001171
5. Chatterjee S, Bhadeshia HKDH (2007) Stretch-flangeability of strong multiphase steels. Mater Sci Technol. https://doi.org/10.1179/174328407X179511
6. Hance BM (2016) Advanced high strength steel: deciphering local and global formability. Proc International Automotive Body Congress Dearborn, Michigan, USA
7. Heibel S, Dettinger T, Nester W, Clausmeyer T, Tekkaya AE (2018) Damage mechanisms and mechanical properties of high-strength multiphase steels. Materials. https://doi.org/10.3390/ma11050761
8. Larour P, Freudenthaler J, Pauli H, Kerschbaum M, Wagner L, Felbinger A, Sonnleitner F, Angeli J (2021) Local formability assessment of AHSS steels with shear cut tensile tests. IOP Conf Ser Mater Sci Eng. https://doi.org/10.1088/1757-899X/1157/1/012054
9. Fang X, Fan Z, Ralph B, Evans P, Underhill R (2003) The relationships between tensile properties and hole expansion property of C-Mn steels. J Mater Sci. https://doi.org/10.1023/A:1025913123832
10. Yoon JI, Jung J, Lee HH, Kim GS, Kim HS (2016) Factors governing hole expansion ratio of steel sheets with smooth sheared edge. Met Mater Int. https://doi.org/10.1007/s12540-016-6346-5
11. Adamczyk RD, Michal GM (1986) Sheared edge extension of high-strength cold-rolled steels. J Appl Metalwork. https://doi.org/10.1007/BF02834379
12. Comstock RJ, Scherrer DK, Adamczyk RD (2006) Hole expansion in a variety of sheet steels. J Mater Eng Perform. https://doi.org/10.1361/105994906X150830
13. Paul SK (2014) Non-linear correlation between uniaxial tensile properties and shear-edge hole expansion ratio. J Mater Eng Perform. https://doi.org/10.1007/s11665-014-1161-y
14. Larour P, Hinterdorfer J, Wagner L, Freudenthaler J, Grünsteidl A, Kerschbaum M (2022) Stretch flangeability of AHSS automotive grades versus cutting tool clearance, wear, angle and radial strain

gradients. IOP Conf Ser Mater Sci Eng 1238012041. https://doi.org/10.1088/1757-899X/1238/1/012041
15. Al-Furjan MSH, Hatami A, Habibi M, Shan L, Tounsi A (2021) On the vibrations of the imperfect sandwich higher-order disk with a lactic core using generalize differential quadrature method. Comp Struct. https://doi.org/10.1016/j.compstruct.2020.113150
16. Al-Furjan MSH, Habibi M, Ghabussi A, Safarpour H, Safarpour M, Tounsi A (2021) Non-polynomial framework for stress and strain response of the FG-GPLRC disk using three-dimensional refined higher-order theory. Eng Struct. https://doi.org/10.1016/j.engstruct.2020.111496
17. Al-Furjan MSH, Habibi M, Ni J, Jung DW, Tounsi A (2022) Frequency simulation of viscoelastic multi-phase reinforced fully symmetric systems. Eng Comput. https://doi.org/10.1007/s00366-020-01200-x
18. Huang X, Hao H, Oslub K, Habibi M, Tounsi A (2022) Dynamic stability/instability simulation of the rotary size-dependent functionally graded microsystem. Eng Comput. https://doi.org/10.1007/s00366-021-01399-3
19. Vinh PV, Chinh NV, Tounsi A (2022) Static bending and buckling analysis of bi-directional functionally graded porous plates using an improved first-order shear deformation theory and FEM. Eur J Mech A Solids. https://doi.org/10.1016/j.euromechsol.2022.104743
20. Kuwabara T, Hashimoto K, Iizuka E, Yoon JW (2011) Effect of anisotropic yield functions on the accuracy of hole expansion simulations. J Mater Process Technol. https://doi.org/10.1016/j.jmatprotec.2010.10.025
21. Iizuka E, Hashimoto K, Kuwabara T (2014) Effects of anisotropic yield functions on the accuracy of forming simulations of hole expansion. Procedia Eng. https://doi.org/10.1016/j.proeng.2014.10.346
22. Kuwabara T, Mori T, Asano M, Hakoyama T, Barlat F (2017) Material modeling of 6016-O and 6016-T4 aluminum alloy sheets and application to hole expansion forming simulation. Int J Plast. https://doi.org/10.1016/j.ijplas.2016.10.002
23. Lee JY, Lee KJ, Lee MG, Kuwabara T, Barlat F (2019) Numerical modeling for accurate prediction of strain localization in hole expansion of a steel sheet. Int J Solids Struct. https://doi.org/10.1016/j.ijsolstr.2018.08.005
24. Korkolis YP, Brownell B, Coppieters S, Tian H (2016) Modeling of hole-expansion of AA6022-T4 aluminum sheets with anisotropic non-quadratic yield functions. J Phys Conf Ser. https://doi.org/10.1088/1742-6596/734/3/032083
25. Ha J, Korkolis YP (2021) Hole-expansion: sensitivity of failure prediction on plastic anisotropy modeling. J Manuf Mater Process. https://doi.org/10.3390/jmmp5020028
26. Chung K, Ma N, Park T, Kim D, Yoo D, Kim C (2011) A modified damage model for advanced high strength steel sheets. Int J Plast. https://doi.org/10.1016/j.ijplas.2011.01.007
27. Takuda H, Ozawa K, Hama T, Yoshida T, Nitta J (2009) Forming limit prediction in bore expansion by combination of finite element simulation and ductile fracture criterion. Mater Trans. https://doi.org/10.2320/matertrans.P-M2009817
28. Yoon JI, Jung J, Kim JG, Sohn SS, Lee S, Kim HS (2017) Key factors of stretch-flangeability of sheet materials. J Mater Sci. https://doi.org/10.1007/s10853-017-1012-y
29. Chinara M, Paul SK, Chatterjee S, Mukherjee S (2021) Effect of planar anisotropy on the hole expansion ratio of cold rolled DP590 steel. Trans Indian Inst Met. https://doi.org/10.1007/s12666-021-02444-x
30. Mu L, Wang Y, Zang Y, Malaquias P, Stemler A (2017) Edge fracture prediction using uncoupled ductile fracture models for DP780 sheet. J Fail and Preven. https://doi.org/10.1007/s11668-017-0245-z
31. Lou Y, Huh H, Lim S, Pack K (2012) New ductile fracture criterion for prediction of fracture forming limit diagrams of sheet metals. Int J Solids Struct. https://doi.org/10.1016/j.ijsolstr.2012.02.016
32. Oh SI, Chen CC, Kobayashi S (1979) Ductile fracture in axisymmetric extrusion and drawing-part 2: workability in extrusion and drawing. J Eng Ind. https://doi.org/10.1115/1.3439471
33. Brozzo P, DeLuca B, Rendina R (1972) A new method for the prediction of formability in metal sheets. Proceedings of the 7th Biennial Conference of IDDRG on Sheet Metal Forming and Formability. Amsterdam, Netherlands
34. Hill R (1948) A theory of the yielding and plastic flow of anisotropic metals. Proc R Soc London Ser A 193A. https://doi.org/10.1098/rspa.1948.0045
35. Kilic S, Ozturk F, Toros S (2019) Analysis of yield criteria and flow curves on FLC for TWIP900 steels. Exp Tech. https://doi.org/10.1007/s40799-020-00382-9
36. Caminero MA (2015) Experimental study of the evolution of plastic anisotropy in 5754 Al-Mg cold rolled sheets. Exp Tech. https://doi.org/10.1111/j.1747-1567.2012.00870.x
37. Soare S, Yoon JW, Cazacu O (2008) On the use of homogeneous polynomials to develop anisotropic yield functions with applications to sheet forming. Int J Plast. https://doi.org/10.1016/j.ijplas.2007.07.016
38. Sener B, Kilicarslan ES, Firat M (2020) Modelling anisotropic behavior of AISI 304 stainless steel sheet using a fourth-order polynomial yield function. Proc Manuf. https://doi.org/10.1016/j.promfg.2020.04.320
39. Sener B, Esener E, Firat M (2021) Modeling plastic anisotropy evolution of AISI 304 steel sheets by a polynomial yield function. SN Appl Sci. https://doi.org/10.1007/s42452-021-04206-2
40. Kovalewski L, Gajewski M (2019) Assessment of optimization methods used to determine plasticity parameters based on DIC and back calculation methods. Exp Tech. https://doi.org/10.1007/s40799-018-00298-5
41. Freudenthal AM (1950) The Inelastic Behavior of Engineering materials and structures. John Wiley and Sons Inc., New York. https://doi.org/10.1017/S0368393100124514
42. Aksen TA, Sener B, Firat M (2020) Failure prediction capability of generalized plastic work criterion. Proc Manuf. https://doi.org/10.1016/j.promfg.2020.04.190
43. Bai Y, Wierzbicki T (2010) Application of extended Mohr-Coulomb criterion to ductile fracture. Int J Fract. https://doi.org/10.1007/s10704-009-9422-8
44. Li Y, Luo M, Gerlach J, Wierzbicki T (2010) Prediction of shear-induced fracture in sheet metal forming. J Mater Process Technol. https://doi.org/10.1016/j.jmatprotec.2010.06.021
45. Luo M, Wierzbicki T (2010) Numerical failure analysis of a stretch-bending test on dual-phase steel sheets using a phenomenological fracture model. Int J Solids Struct. https://doi.org/10.1016/j.ijsolstr.2010.07.010
46. Habibi N, Ramazani A, Sundararaghavan V, Prahl U (2018) Failure predictions of DP600 steel sheets using various uncoupled fracture criteria. Eng Fract Mech. https://doi.org/10.1016/j.engfracmech.2017.12.022
47. Alaie A, Kadkhodapour J, Rad SZ, Asadabad MA, Schmauder S (2015) Formation and coalescence of strain localized regions in ferrite phase of DP600 steels under uniaxial tensile deformation. Mater Sci Eng A. https://doi.org/10.1016/j.msea.2014.11.042
48. Aşık EE, Perdahcıoğlu ES, Boogard VD (2019) Microscopic investigation of damage mechanisms and anisotropic evolution of damage in DP600. Mater Sci Eng A. https://doi.org/10.1016/j.msea.2018.10.018
49. Heibel S, Nester W, Clausmeyer T, Tekkaya AE (2016) Damage characterization of high-strength multiphase steels, IOP conf. Ser Mater Sci Eng. https://doi.org/10.1088/1757-899X/159/1/012013
50. ASTME517-19 Standard Test Method for Plastic Strain Ratio r for Sheet Metal. https://doi.org/10.1520/E0517-19
51. Stoughton TB, Shi MF, Huang G, Yoon JW (2014) Material characterizations for benchmark 1 and benchmark 2. Numisheet 2014 AIP Conf Proc. https://doi.org/10.1063/1.4849976
52. Cardoso MC, Moreira LP (2015) : Forming limit analysis of DP600-800 steels. Int J Mat Metal Eng. scholar.waset.org/1307–6892/10002286

53. International Organization for Standardization (ISO) (2009) Technical Specification, Metallic materials – Method of Hole Expanding Test, ISO/TS 16630. https://www.iso.org
54. Levin E, Larour P, Heuse M, Staupendahl D, Clausmeyer T, Tekkaya AE (2018) Influence of cutting tool stiffness on edge formability. IOP Conf Ser Mater Sci Eng. https://doi.org/10.1088/1757-899X/418/1/012061
55. Dieter GE (1988) Mechanical Metallurgy. Third ed., London
56. Qin S, Beese AM (2020) Multiaxial fracture of DP600: experiments and finite element modeling. Mater Sci Eng A. https://doi.org/10.1016/j.msea.2020.139386
57. Kusche CF, Pütz F, Münstermann S, Al-Samman T, Korte-Kerzel S (2021) On the effect of strain and triaxiality on void evolution in a heterogeneous microstructure – a statistical and single void study of damage in DP800 steel. Mater Sci Eng A. https://doi.org/10.1016/j.msea.2020.140332
58. Paul SK (2020) A critical review on hole expansion ratio. Materialia. https://doi.org/10.1016/j.mtla.2019.100566
59. Marc 2018.1 Volume A: Theory and User Manual. https://help.hexagonmi.com/tr-TR/bundle/Marc_2021.4-Volume_A_Theory_and_User_Information/resource/Marc_2021.4-Volume_A_Theory_and_User_Information.pdf
60. Marc 2018.1 Volume B: Element Library. https://help.hexagonmi.com/tr-TR/bundle/Marc_2021.1-Volume_B_Element_Library/resource/Marc_2021.1-Volume_B_Element_Library.pdf
61. Choi SH, Kim EY, Kim SI (2014) The micromechanical deformation behaviors of hot rolled 590FB steel during hole-expansion test. Int J Plast. https://doi.org/10.1016/j.ijplas.2013.11.010
62. Bao Y, Wierzbicki T (2004) On fracture locus in the equivalent strain and stress triaxiality space. Int J Mech Sci. https://doi.org/10.1016/j.ijmecsci.2004.02.006
63. Lou Y, Yoon JW, Huh H (2014) Modeling of shear ductile fracture considering a changeable cut-off value for stress triaxiality. Int J Plast. https://doi.org/10.1016/j.ijplas.2013.08.006
64. Hancock JW, Brown DK (1983) On the role of strain and stress state in ductile failure. J Mech Phys Solids. https://doi.org/10.1016/0022-5096(83)90017-0
65. Paul SK (2019) The effect of deformation gradient on necking and failure in hole expansion test. Manuf Lett. https://doi.org/10.1016/j.mfglet.2019.08.004
66. Bettaieb MB, Meraim FA (2017) Theoretical and numerical investigation of the impact of out-of-plane compressive stress on sheet metal formability. Int J Mech Sci. https://doi.org/10.1016/j.ijmecsci.2017.05.046
67. Liu W, Chen BK, Pang Y, Najafzadeh A (2020) A 3D phenomenological yield function with both in and out-of-plane mechanical anisotropy using full-field crystal plasticity spectral method for modelling sheet metal forming of strong textured aluminum alloy. Int J Solids Struct. https://doi.org/10.1016/j.ijsolstr.2020.02.008
68. Cazacu O (2018) New yield criteria for isotropic and textured metallic materials. Int J Solids Struct (2018). https://doi.org/10.1016/j.ijsolstr.2018.01.036